Peak to Average Power Ratio Reduction Schemes
and
Synchronization Algorithms for OFDM Based Systems

A Project Report
Submitted in Partial Fulfillment of the
Master of Engineering
in Telecommunication

by

SACHIN CHAUDHARI

Project Guide : **Prof. K.V.S.HARI**

Department of Electrical Communication Engineering
Indian Institute of Science
Bangalore-560012
India

July 2004

Acknowledgments

I am greatly indebted to my guide Prof. **K.V.S.Hari** for his help and support throughout the course of this project.

I would like to thank Joby, Bhavani, Vijay, Avinash, Deepak and Abhishek (SSP labmates) for their help and discussions during the course of project. I would like to thank my friends Tanmay, Ajay, Rupesh, Pankaj and Vibhor for giving me a great time at IISc.

I am thankful to my parents, my sister Shweta and my best friend Kiran for their love, and support.

Abstract

The relation of upper bound on Peak to Average Power Ratio (PAPR) with input constellation PAPR is derived for general constellation and it is shown that upper bound on PAPR is greater for QAM as compared to PSK of same order. A "pulse shaping scheme" is proposed for reduction of upper bound on PAPR. An analytical expression for reduction in upper bound is obtained in terms of pulse shaping weights and it is shown that more the variation in weights, more is the reduction.

Interleaved OFDM (IOFDM) was proposed to increase code rate without increasing PAPR. IOFDM is studied from point of view of PAPR reduction while keeping code rate constant. Also IOFDM is shown to be superset of OFDM and Single Carrier Frequency Division Equalization (SC-FDE). IOFDM can be used for trading with respect to number of subcarriers to get best of OFDM and SC-FDE. IOFDM is shown to be better then most of the present scheme in terms of PAPR reduction, complexity, and redundancy added. Block OFDM is proposed and compared with IOFDM to study role of interleaving with regards to complexity.

A simple and efficient scheme "Tone based Integer Frequency Offset (IFO) Estimation" is proposed for IFO estimation. A modification is proposed which improves the performance in ISI case. A detailed mathematical analysis is presented and the expression for Probability of error for most general case is derived. Later it is compared with present algorithms in literature. It is also shown how the proposed scheme is used in conjunction with Schmidl Cox Algorithm (SCA) for overall synchronization and channel estimation in OFDM.

List of Abbreviations

ACI	Adjacent Carrier Interference
AWGN	Additive White Gaussian Noise
BER	Bit Error Rate
BOFDM	Block Orthogonal Frequency Division Multiplexing
CFO	Carrier Frequency Offset
CIR	Channel Impulse Response
CP	Cyclic Prefix
CCDF	Complimentary Cumulative Distribution Function
DFT	Discrete Fourier Transform
FFT	Fast Fourier Transform
FIR	Finite Impulse Response
HPA	High Power Amplifier
IBI	Inter Block Interference
ICI	Inter Carrier Interference
IDFT	Inverse Discrete Fourier Transform
IFFT	Inverse Fast Fourier Transform
IFO	Integer Frequency offset
IOFDM	Interleaved Orthogonal Frequency Division Multiplexing
ISI	Inter Symbol Interference
ML	Maximum Likelihood
MZB	Minn Zeng Bhargava (algorithm)
OFDM	Orthogonal Frequency Division Multiplexing
PAPR	Peak to Average Power Ratio
PN	Pseudo Noise
PSK	Phase Shift Keying
PTS	Partial Transmit Sequence

QAM	Quadrature Amplitude Modulation
QPSK	Quadrature Phase Shift Keying
SC-FDE	Single Carrier Frequency Domain Equalization
SCA	Schmidl Cox Algorithm
SLM	Selected Mapping
SNR	Signal to Noise Ratio

List of Symbols

capital with bold face	Matrix
$(\cdot)^H$	Hermitian
$(\cdot)^T$	Transpose
$(\cdot)^*$	Conjugate
$(\cdot)^{-1}$	Inverse
$\widehat{a}$	Estimate of a
$\underline{a}$	Vector a
$*$	Linear convolution operation
γ_c	Input Constellation PAPR
ϕ	Phase difference between two halves of first training symbol
ϕ_i	Phase of ith subcarrier
τ	Timing Offset
ℓ	Size of correlating block in SCA (and its value is N/2)
ϵ_{frac}	Fractional frequency offset normalized to subcarrier spacing
$\mathcal{N}(\mu, \sigma^2)$	Gaussian random variable with mean μ and variance σ^2
$\mathbf{0}_N$	$N \times N$ zero matrix
$\mathbf{I}_N$	$N \times N$ identity matrix
$\triangle f$	Actual frequency offset
$\triangle k$	Frequency offset normalized to subcarrier spacing
$\triangle k_i$	Integer Frequency Offset
$b_n^{(v)}$	v^{th} rotation factor in PTS-OFDM
$\underline{c}$	pulse shaping vector in Proposed Pulse Shaping Scheme
$\underline{d}^{(u)}$	u^{th} rotation vector in SLM-OFDM
k	Subcarrier index (Discrete Frequency Domain)
k_i	Index of subcarrier on which data corresponding to IFO training symbol is send

k_i'	Index of subcarrier on which data corresponding to IFO training symbol is expected after occurrence of IFO at receiver
m	Number of subcarriers on which data is send in IFO training symbol of proposed scheme.
n	Corresponds to n^{th} block
$\underline{s}$	$N \times 1$ Input vector to IFFT at the transmitter
t	Discrete time index
t_c	Continuous time index
$w(t)$	AWGN
$\underline{x}$	$N \times 1$ Output vector of IFFT at transmitter
$\underline{y}$	i. In chapter 2,3,4, and 5, $M \times 1$ received vector at receiver.
	ii. In chapter 6 and 7, $N \times 1$ vector input to FFT at receiver
$B(g)$	Metric for IFO estimation in SCA
$C(k)$	Metric for IFO estimation in proposed scheme (Tone based)
$\mathbf{C_{pk}}$	$PK \times PK$ Precoding block diagonal matrix in IOFDM ($N = PK$)
$\mathbf{D}$	Diagonal matrix with (k,k) entry as channel transfer function for k^{th} subcarrier
$\mathbf{F}_N$	$N \times N$ point FFT matrix
F_{sp}	Subcarrier spacing
$F_r(x)$	CDF of random variable r
$\mathbf{G^{-1}}$	$PK \times PK$ Preprocessing Block diagonal matrix in IOFDM
$\mathbf{H}_0$	$M \times M$ channel convolution matrix
$\mathbf{H}_1$	$M \times M$ Inter block interference matrix
$H(k)$	Channel transfer function value at k^{th} subcarrier
$\tilde{\mathbf{H}}$	$N \times N$ Circulant matrix with entry as $h(n-k))$
K	Number of subcarrier in IOFDM
L	Upperbound on channel order
$\mathbf{L}_i$	$PK \times PK$ Interleaving matrix
$\mathbf{L_{pk}}$	$PK \times PK$ Permutation matrix
M	Length of total OFDM symbol after CP addition
$M(d)$	Timing metric for SCA at d^{th} instant
N	Number of Subcarriers in OFDM
Ng	Length of Cyclic Prefix
P	Interleaving Factor in IOFDM
P_i	Instantaneous PAPR

P_s	Average power of OFDM symbol (excluding CP)
Pc	Probability of correct estimation of IFO
Pe	Probability of error in estimation of IFO
Pe_{sm}	Pe when data is sent on m subcarriers in proposed scheme for IFO estimation
P_w	Worst case PAPR
$P_{w_{ck}}$	Worst case PAPR for given value of $\underline{c}$ in Pulse Shaping Scheme for PAPR
$\mathbf{R_{cp}}$	$N \times M$ Cyclic prefix removal matrix
Sm	Case of Proposed scheme in which data has been sent on m subcarriers and zeroes on rest of the subcarriers
T	Time duration of OFDM symbol (without CP)
T_s	Time duration of one input symbol to IDFT
$\mathbf{T_{cp}}$	$M \times N$ Cyclic prefix addition matrix
U	Number of distinct pseudo random, but fixed vector in SLM-OFDM
V	Number of pairwise disjoint blocks in PTS-OFDM
W_a	Number of allowed phase angle in PTS-OFDM
$Y(k)$	DFT of $y(t)$ at receiver for chapter 6, and 7
$W(k)$	DFT of $w(t)$ at receiver for chapter 6, and 7
$W_1(k)$	Cyclically shifted $W(k)$

Contents

List of Figures

List of Tables

Chapter 1

Introduction

1.1 OFDM

Orthogonal Frequency Division Multiplexing (OFDM) is a parallel data system. In OFDM [1],[2], the wide band channel is divided into number of subchannels. These subchannels are permitted to overlap in frequency domain with specific orthogonality constraints imposed to facilitate separation of subchannels at the receiver. The serial data symbols are divided into parallel streams, then modulating each parallel stream onto a separate subchannel. The symbol rate on each subchannel is lower than overall symbol rate. Due to lower symbol rate on each subchannel, each subchannel looks like a flat fading channel. OFDM has the advantage of spreading out the burst errors caused by additive burst noise randomly so that the distortion of several adjacent symbols is avoided. OFDM has the additional advantage of spreading out the symbol interval thereby reducing the ISI caused due to delay spread. Therefore OFDM is an effective technique for combating multipath fading and for high data rate transmission.

1.2 Motivation for Present Work

1.2.1 PAPR

Due to large number of subcarriers, the OFDM signal has large dynamic range with large Peak to Average Power Ratio (PAPR). When considering a system with transmitting power amplifier, the non-linear distortions and peak amplitude limiting introduced by the High Power Amplifier (HPA) will produce intermodulation between the different carriers and introduce additional interference into the system. This additional interference leads to an increase in Bit Error Rate (BER) of the system. One way to avoid such non-linear distortions and keep a low BER is by forcing the amplifier to work in its linear region. Unfortunately such solution is not power efficient and thus not suitable for wireless communications.

Hence there is need for reducing PAPR of transmitted signal. Several techniques have appeared

in literature [11] to [21] and few are proposed.

1.2.2 Synchronization

Synchronization is an important step that must be performed at the receiver in OFDM systems, before an OFDM receiver starts demodulating subcarriers. Synchronization of an OFDM signal requires finding the symbol timing and carrier frequency offset. Symbol timing for an OFDM is significantly different than for a single carrier signal, since there is not an "eye opening" where a best sampling time can be found. Rather there are hundreds of samples per OFDM symbol as number of samples is directly proportional to number of subcarriers. There is some tolerance for symbol timing errors when a cyclic prefix is used to extend the symbol. But synchronization of carrier frequency at the receiver must be done accurately, failing which, there will be loss of orthogonality between subcarriers resulting in performance degradation.

Many papers on the subject of synchronization for OFDM have appeared in literature [22] to [27] in recent years. A scheme has been proposed for integer frequency offset.

1.3 Contribution of this project

1.3.1 PAPR

1. The dependency of PAPR on input constellation (through γ_c) is shown and corresponding expression for P_w is obtained for general constellation.

2. A new scheme, called "Pulse Shaping Scheme", is proposed for PAPR reduction. An analytical expression for reduction in upperbound of PAPR is obtained in terms of pulse shaping weights.

3. IOFDM is reviewed from PAPR reduction point of view for constant code rate. Also it is shown that IOFDM is superset of OFDM and Single Carrier Frequency Domain Equalization (SC-FDE). IOFDM is compared with some of the schemes present in literature.

4. Block OFDM is proposed which has similar structure to that of IOFDM (but without interleaving and minor differences). It is shown that BOFDM is also superset of OFDM and SC-FDE. Performance comparison of BOFDM and IOFDM is carried out.

1.3.2 Synchronization

1. A new scheme, called " Tone based Integer Frequency Offset estimation", is proposed for Integer Frequency Offset Estimation. Modification was suggested for the proposed scheme which greatly improves the performance of the proposed scheme. A detailed mathematical analysis has been presented and Probability of error (Pe) expression for ISI and AWGN channel has been derived. The proposed scheme is compared with other scheme in literature. Later it is shown that the proposed scheme is used effectively with the existing algorithm called Schmidl

Cox Algorithm for overall synchronization i.e. timing, fractional frequency offset and integer frequency offset.

1.4 Organization of Project Report

The project report is organized as follows. In chapter 2, conventional OFDM is described. In chapter 3, PAPR is introduced and factors affecting PAPR are discussed in detail. Some PAPR reduction schemes are also discussed in the same chapter. In chapter 4, Interleaved OFDM and Single Carrier Frequency Domain Equalization systems are discussed. In Chapter 5, issues regarding Synchronization are discussed followed with the discussion on existing Synchronization Scheme. In chapter 6, a scheme is proposed for Integer Frequency Offset (IFO) estimation and compared with existing scheme. Chapter 7 concludes the current work.

Chapter 2

OFDM

2.1   Generation of OFDM signal

An OFDM signal consists of sum of subcarriers that are modulated by using phase shift keying (PSK) or quadrature amplitude keying (QAM). N number of such symbols are then fed to IDFT through serial to parallel converter where N is number of subcarriers. If $s_0, s_1, \ldots, s_{N-1}$ are N complex QAM (or PSK) symbols, then output of the IDFT are

$$x(t) = \frac{1}{\sqrt{N}} \sum_{k=0}^{N-1} s_k e^{\frac{j2\pi tk}{N}} \qquad t = 0, 1, \ldots, N-1 \tag{2.1}$$

They are then converted to serial stream by parallel to serial (P/S) converter. The block of N output symbols from parallel to serial converter make up one OFDM symbol. If T_s is the time duration of one input symbol to IDFT, then the total duration of a single OFDM symbol is $T = NT_s$.

Note that the sinusoids of the DFT (or IDFT) form an orthogonal basis set and a signal in vector space of the DFT (or IDFT) can be represented as linear combination of the orthogonal sinusoids. Thus the IDFT at the transmitter maps an input signal onto a set of orthogonal subcarriers. Similarly the transform DFT is used at the receiver to reverse the mapping of IDFT and signal from the subcarriers are combined to form an estimate of the source signal from the transmitter. Since the basis function of DFT are uncorrelated, the correlation performed in DFT for the given subcarrier only sees energy for that corresponding subcarrier. The energy from other subcarrier does not contribute because they are uncorrelated. This separation of signal energy is the reason that OFDM subcarriers spectrum can overlap without causing interference.

In practice OFDM systems are implemented using a combination of Fast Fourier Transform (FFT) and Inverse Fast Fourier Transform (IFFT) that are mathematically equivalent versions of the DFT and IDFT, but are computationally more efficient. Complexity of DFT is N^2 whereas that of FFT is $\frac{N}{2} log N$.
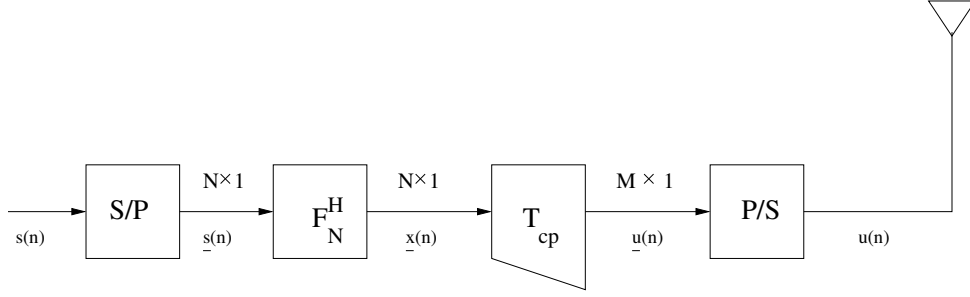
Figure 2.1: OFDM Transmitter

2.2 OFDM system

Figure 2.1 shows a discrete time baseband model of an OFDM transmitter. At the transmitter the bit stream is mapped onto a complex symbol $s(n)$ using any modulation scheme. The symbol stream is then blocked into a parallel block stream $\underline{s}(n)$, each block comprising N symbols so that we have $\underline{s}(n) = [s(nN), s(nN + 1), \ldots\ldots, s(nN + N - 1)]^T$. Here n denote the block index. The block stream $\underline{s}(n)$ is then precoded using $N \times N$ point IFFT matrix $\mathbf{F}_N^H$ to yield so called time domain block vector $\underline{x}(n)$. Then redundancy of length N_g is added to each block using cyclic prefix (N_g is length of Cyclic prefix and $N_g \geq L$, where L is upperbound on channel order). The entries of the resulting block are $\underline{u}(n) = [u(nM), u(nM + 1), \ldots, u(nM + M - 1)]^T$, where $M = N + Ng$. This block is then transformed to serial stream $u(n)$, upconverted to RF and is transmitted through antenna.

The following equations represent the precoding and cyclic prefix (CP) insertion operation :

$$\underline{x}(n) \quad = \quad \mathbf{F}_N^H \, \underline{s}(n) \tag{2.2}$$

$$\underline{u}(n) \quad = \quad \mathbf{T_{cp}} \, \underline{x}(n) \tag{2.3}$$

where $\mathbf{T_{cp}}$ is $M \times N$ matrix given by $\mathbf{T_{cp}} = [\mathbf{F_{cp}}, \mathbf{F}]^H$, $\mathbf{F_{cp}}$ is $N \times N_g$ matrix formed by the last N_g rows of $\mathbf{F}_N$. The frequency selective propagation can modeled as an FIR filter with the channel impulse response (CIR) column vector $\underline{h} = [h_0, h_1, \ldots, h_L]^T$ and additive white gaussian noise $\underline{w}(n)$ of variance σ^2. We assume that we have perfect knowledge of CIR at the receiver and no CIR is available at the transmitter.

Letting $\underline{y}(n)$ be the nth received block, with $\underline{y}(n)$ being the signal at the receiver front end after downconversion from RF and blocking from serial to parallel, we can represent the transmit receive equations as

$$\underline{y}(n) \quad = \quad \mathbf{H_0} \, \underline{u}(n) + \mathbf{H_1} \, \underline{u}(n - 1) + \underline{w}(n) \tag{2.4}$$

where $\mathbf{H_0}$ is $M \times M$ lower triangular Toeplitz filtering matrix given as

$$\mathbf{H_0} = \begin{pmatrix} h(0) & 0 & 0 & \ldots & 0 \\ \vdots & h(0) & 0 & \ldots & 0 \\ h(L) & \ldots & \ddots & \ldots & \vdots \\ \vdots & \ddots & \ldots & \ddots & 0 \\ 0 & \ldots & h(L) & \ldots & h(0) \end{pmatrix}$$

and $\mathbf{H_1}$ represent Inter-Block Interference (IBI) $M \times M$ upper triangular Toeplitz filtering matrix given by

$$\mathbf{H_1} = \begin{pmatrix} 0 & \ldots & h(L) & \ldots & h(1) \\ \vdots & \ddots & 0 & \ddots & 0 \\ 0 & \ldots & \ddots & \ldots & h(L) \\ \vdots & \vdots & \vdots & \ddots & \vdots \\ 0 & \ldots & 0 & \ldots 0 & 0 \end{pmatrix}$$

and $\underline{w}(n) = [w(nM), \ldots, w(nM + M - 1)]^T$ denotes AWGN vector. At the receiver, cyclic prefix is removed by using receive matrix $\mathbf{R_{cp}} = [\mathbf{0}_{N \times N_g} \ \mathbf{I}_N]$ to give IBI free block given by

$$\begin{aligned} \hat{\underline{x}}(n) &= \mathbf{R_{cp}} \, \underline{y}(n) & (2.5) \\ &= \mathbf{R_{cp}} \, \mathbf{H_0} \, \mathbf{T_{cp}} \, \underline{x}(n) + \mathbf{R_{cp}} \, \underline{w}(n) & (2.6) \end{aligned}$$

Note that IBI inducing matrix has been eliminated by $\mathbf{R_{cp}}$ (from equations 2.4,2.6, and $\mathbf{R_{cp}}\mathbf{H_1} = \mathbf{0}_{N \times M}$). Thus redundancy is used to mitigate multipath effectively. Now $\widetilde{\mathbf{H}} = \mathbf{R_{cp}}\mathbf{H_0}\mathbf{T_{cp}}$ is $N \times N$ circulant matrix with its (n,k) entry as $h((n - k) mod N)$. This shows that by inserting CP (through $\mathbf{T_{cp}}$ matrix) and removing it at the receiver (using $\mathbf{R_{cp}}$), the linear convolution channel with IBI is converted to circular one without IBI. Therefore equation 2.6 becomes

$$\hat{\underline{x}}(n) = \widetilde{\mathbf{H}}\underline{x}(n) + \mathbf{R_{cp}}\underline{w}(n) \qquad (2.7)$$

Equalization of OFDM with CP transmission relies on following important property of circulant matrix

Diagonalization of circulant matrices : An $N \times N$ circulant matrix $\widetilde{\mathbf{H}}$ can be diagonalized by pre and post multiplication with FFT and IFFT matrices of size N i.e.
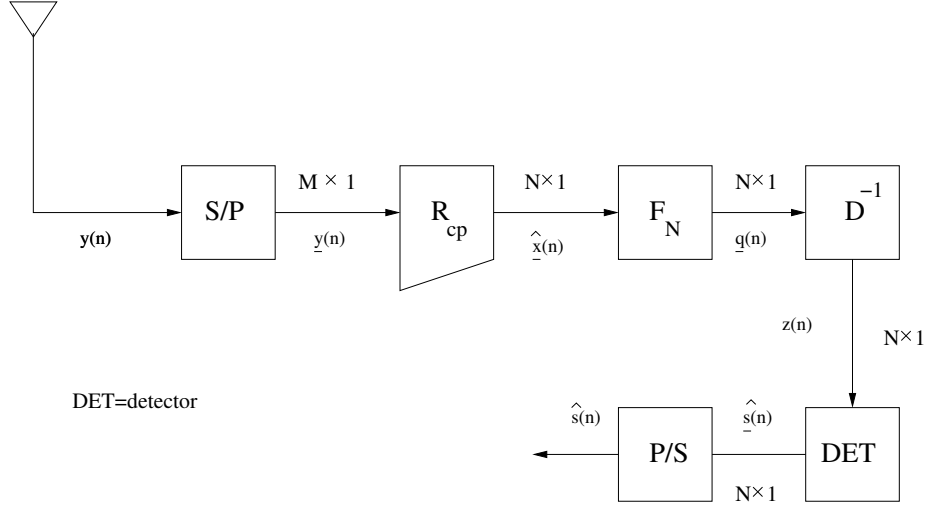
Figure 2.2: OFDM Receiver

$$\mathbf{F}_N\widetilde{\mathbf{H}}\mathbf{F}_N^H = \mathbf{D} \tag{2.8}$$

where $\mathbf{D} = diag[H_0, H_1, \ldots\ldots, H_{N-1}]$ with $H_k = H(k) = \sum_{l=0}^{L} h_l e^{-2\pi kl/N}$ denoting the channel transfer function for the kth subcarrier. Note $\mathbf{D}$ is $N \times N$ matrix. $\square$

Now equation 2.7 can be written as

$$\hat{\underline{x}}(n) = \mathbf{F}_N^H\mathbf{D}\mathbf{F}_N\underline{x}(n) + \mathbf{R_{cp}}\underline{w}(n) \tag{2.9}$$

Taking FFT of both sides and noting that $\underline{x} = \mathbf{F}_N^H\underline{s}(n)$ gives

$$\underline{q}(n) = \mathbf{D}\underline{s}(n) + \mathbf{F}_N\mathbf{R_{cp}}\underline{w}(n) \tag{2.10}$$

Taking $\mathbf{D}^{-1}$ (assuming $\mathbf{D}$ is invertible which is possible if and only if the channel transfer function does not have zero on FFT grid i.e. $H_k \neq 0 \quad \forall\, k \in [0, N-1]$), we get

$$\underline{z}(n) = \underline{s}(n) + \mathbf{D}^{-1}\mathbf{F}_N\mathbf{R}_{cp}\underline{w}(n) \tag{2.11}$$

Finally passing $\underline{z}(n)$ through the detector we get $\hat{\underline{s}}(n)$, approximation to $\underline{s}(n)$. Receiver diagram is shown in figure 2.2.

2.3 Important Remarks

1. We can use Zero Padding [1],[9],[10] instead of cyclic prefix at the transmitter, and do overlap add operation at the receiver, the same transformation of the channel convolution matrix from a toeplitz to circulant is obtained. One difference between cyclic prefix and the zero pad is that the redundancy in case of cyclic prefix is data dependent, while in case of zero padding it is data independent and hence can be used for channel estimation. Moreover if one does not discard the zero pad at the receiver, the equivalent channel convolution matrix is tall Toeplitz which is guaranteed to be full rank as long as all of the channel taps are not zero. This system is resistant to channel nulls.

2. The role of IFFT at the transmitter can also be interpreted thus : The modulated individual OFDM subcarriers can be viewed as the spectrum of the signal to be transmitted and hence one needs an IFFT to transform the 'spectrum' to time domain to transmit it through channel.

3. The equalized signal/decision vector is given by equation 2.11. It can be seen that the noise vector is multiplied by the inverse of the diagonal matrix $\mathbf{D}$, comprising the eigenvalues of the equivalent channel convolution matrix $\widetilde{\mathbf{H}}$. If one or more eigenvalues are close to zero, then the noise will be amplified. In other words, the channel must not have zeros on any of the subcarriers.

4. The code rate of the OFDM system is the ratio between the number of useful symbols to the total number of symbols transmitted. Hence the code rate is given by $\frac{N}{N+N_g}$. The number of redundant symbol is greater than equal to upperbound on the length of CIR.

5. OFDM works with the assumption that the CIR does not change in the time required to transmit $N + N_g$ symbols. If the CIR changes within this time, then the equalization will not work at the receiver and the block of $N + N_g$ symbols will be lost.

Chapter 3

PAPR

3.1 Introduction

An OFDM signal consists of number of independently modulated subcarriers, which can give large peak to average power ratio (PAPR) when added up coherently. When N signals are added with the same phase they produce a peak power that is N times their average power. This effect is illustrated in figure 3.1 for $N = 16$ case, for which the peak power is 16 times the average value. A large PAPR brings disadvantage like an increased complexity of the analog to digital and digital to analog converters and reduced efficiency of the RF power amplifier.

From equation 2.1 we know that OFDM signal (block of N symbols) is generated using input symbols $s(k)$, $k = 0, 1, \ldots, N - 1$ as

$$x(t) \quad = \quad \frac{1}{\sqrt{N}} \sum_{k=0}^{N-1} s(k) e^{j2\pi kt/N} \qquad t = 0, 1, \ldots, N - 1 \tag{3.1}$$

Note that this definition of IFFT does not scale the input power i.e total input and output power of IFFT are same. Same is the case with average input power and average output power of IFFT. Throughout the report this normalized definitions are used for IFFT and FFT. Now instantaneous PAPR for above case can be given by

$$P_i \quad = \quad \frac{\max_t |x(t)|^2}{E[|x(t)|^2]} \tag{3.2}$$

3.2 Distribution of PAPR

Assume that $s(k)$ are from QPSK, i.e. $s(k) \in \{-1, 1, j, -j\}$. From the central limit theorem it follows that for large values of N, the real and imaginary values of $x(t)$ becomes Gaussian distributed,
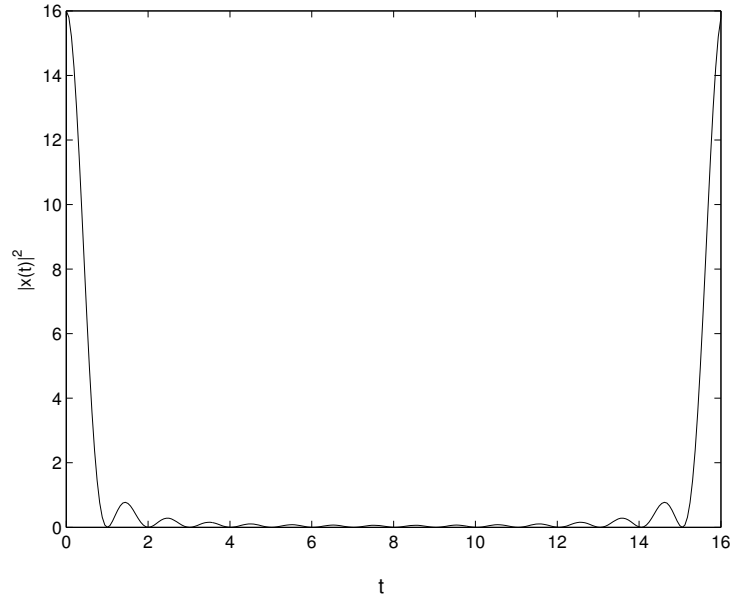
Figure 3.1: Plot of signal power of IFFT output for 16 channel OFDM signal, modulated with same initial phase for all subchannels and average power=1

each with variance 0.5. The amplitude of the OFDM signal therefore has a Rayleigh distribution while the power distribution becomes Central chi-square distribution with two degrees of freedom and zero mean with cumulative distribution given by

$$F(z) \;\; = \;\; 1 - e^{-z} \tag{3.3}$$

We want complementary cumulative distribution (CCDF) function for the peak power per OFDM symbol. Assuming the samples are mutually uncorrelated, the probability that PAPR P_i is above some threshold level can be written as

$$
\begin{aligned}
P(P_i > z) \;\; &= \;\; 1 - F(z)^N \\
&= \;\; 1 - (1 - e^{-z})^N
\end{aligned}
\tag{3.4}
$$

The CCDF for N=16, 32, 64, 128 is plotted in figure 3.2.

The distribution of PAPR illustrates that symbols with high PAPR occurs less frequently. So it is possible to deduce coding techniques to reduce PAPR by transmitting symbols with low PAPR only. A different way to solve the PAPR problem is to remove the peaks at the cost of slight interference that can be made as small as possible. Many schemes are based on bending the CCDF curves toward left, and thus further reduce the probability of occurring of symbols with high PAPR. Some of them
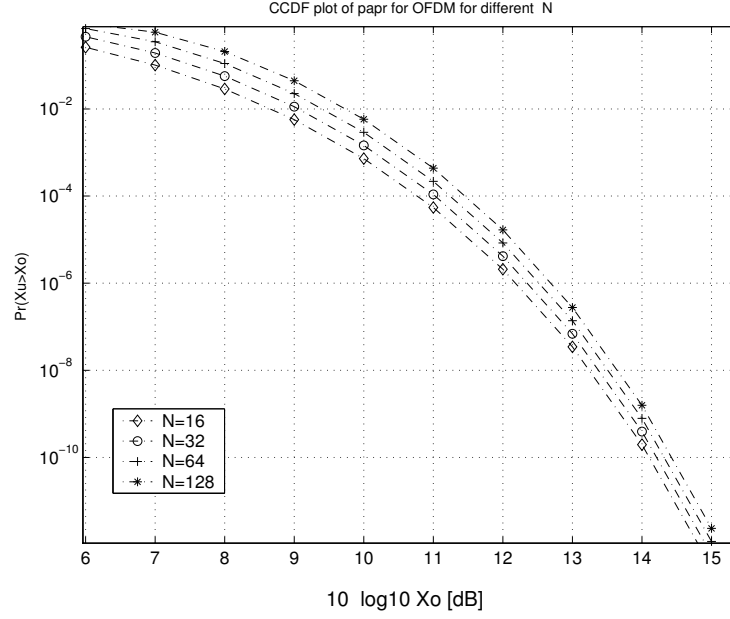
Figure 3.2: CCDF for N=16, 32, 64, 128

are discussed later in this chapter (for example, Selected Mapping, Partial Transmit Sequences).

3.3   Factors Affecting PAPR

Before discussing the factors affecting PAPR, we will derive upperbound on P_i. We call it worst case PAPR and denote it by P_w. From equation 3.2

$$
\begin{aligned}
P_i &= \frac{max_t|\,x(t)|^2}{E[\,|x(t)|^2]} = \frac{max_t\frac{1}{N}|\sum_{k=0}^{N-1}s(k)e^{j2\pi kt/N}\,|^2}{E[\,|s(k)|^2]} \\[2mm]
&\leq \max_t \frac{\sum_{k=0}^{N-1}|s(k)e^{j2\pi kt/N}\,|^2}{E[\,|s(k)|^2]} \qquad \because |\sum_{k=0}^{N-1}a_n|^2 \leq N\sum_{k=0}^{N-1}|a_n|^2 \\[2mm]
&= \frac{\sum_{k=0}^{N-1}|s(k)|^2}{E[\,|s(k)|^2]} \\[2mm]
&\leq \max_k \frac{N\,|s(k)|^2}{E[\,|s(k)|^2]}
\end{aligned}
\tag{3.5}
$$

Therefore P_w is given by

$$
P_w = \max_k \frac{N\,|s(k)|^2}{E[\,|s(k)|^2]}
\tag{3.6}
$$

Let us define γ_c as

$$\gamma_c = \max_k \frac{|s(k)|^2}{E[|s(k)|^2]} \tag{3.7}$$

It can be seen from the above equation that γ_c is nothing but PAPR of the input constellation, so that equation 3.6 can be written as

$$P_w = N\gamma_c \tag{3.8}$$

Important factors on which PAPR depends are

1. N, number of subcarriers in OFDM system :

PAPR depends linearly on N (from equation 3.8). If we reduce N then PAPR reduces, but code rate also decreases (assuming channel order remains constant).

2. γ_c , Input constellation PAPR :

PAPR is directly proportional to γ_c (from equation 3.8). It is straight forward that γ_c is more for QAM as compared to PSK. In fact for **any order** PSK $\gamma_c = 1$. In case of QAM, γ_c increases with increasing order. So that we can write

$$P_{qam} = \gamma_{qam} P_{psk} \tag{3.9}$$

where P_{qam} is P_w for QAM, P_{psk} is P_w for PSK, and γ_{qam} is γ_c for QAM. In fact, the above equation is true for arbitrary constellation given that they are fed the same sequences. Henceforth we will use only PSK for discussion on PAPR.

3. Autocorrelation of data sequences :

To see dependence of PAPR on out of phase aperiodic autocorrelation values on data sequences, we state a theorem [11].

Theorem : Let the aperiodic autocorrelation coefficient be

$$\rho(l) = \sum_{k=1}^{N-k} s(k+l)s^*(k) \quad for\ k = 0, 1, \ldots, N-1$$

with $|s(k)|^2 = 1\ \forall k$, then the peak factor is upper bounded by

$$P_i \leq 1 + \frac{2}{N} \sum_{l=1}^{N-1} |\rho(l)| \qquad \square \tag{3.10}$$

From this equation 3.10, P_w for a allowed set of input sequences is given by

$$P_w \quad = \max_{\underline{s}}(\quad 1 + \frac{2}{N} \sum_{l=1}^{N-1} |\rho(l)|) \tag{3.11}$$

This dependence of PAPR on autocorrelation of data sequence is exploited to reduce the PAPR by using the sequences that have low autocorrelation coefficient for $k \neq 0$. For example, Golay sequences have been extensively used for reduction of PAPR and are discussed in next chapter. In fact equation 3.8 is special case of equation 3.10 with $\rho(l) = 1 \ \forall \, k = 0, 1, \ldots, N-1$.

3.4   PAPR Reduction Schemes

Several techniques [11]-[21] have been proposed for reducing PAPR. Some of them are discussed in this chapter. The important factors while looking at different schemes are complexity, redundancy, and reduction in PAPR.

3.4.1   Signal Distortion Techniques

This technique reduce the peak amplitude simply by nonlinearly distorting the OFDM signal at or around the peaks. Examples of distortion techniques are clipping, peak windowing and peak cancellation. The disadvantage is that by distorting the OFDM signal amplitude, a kind of self interference is introduced, that degrades bit error rate (BER). Second disadvantage is that the nonlinear distortion increases the level of out of band radiation. Details can be found in [2]. Their mention here is for sake of completeness. Our main focus of the section will be on techniques that avoid or reduce the occurrence of symbols with high PAPR. It is rightly said " Prevention is Better than Cure".

3.4.2   Selected Mapping

In a more general approach [14],[15], it is assumed that U statistically independent alternative transmit sequences $\underline{x}_n^{(u)}$ represent the same information (n denotes n^{th} block). Then the one with lowest PAPR (denoted as $\mathcal{X}_n$) is selected for transmission. The probability that $\mathcal{X}_n$ exceeds threshold PAPR ($\mathcal{X}_o$) is approximately

$$Pr\{\mathcal{X}_n > \mathcal{X}_o\} \quad = \quad (1 - (1 - e^{-\mathcal{X}_o})^N)^U \tag{3.12}$$

Because of the selected assignment of binary data to transmit signal, this principle is called selected mapping.The block diagram of SLM-OFDM (Selected Mapping OFDM) is shown in figure 3.3.
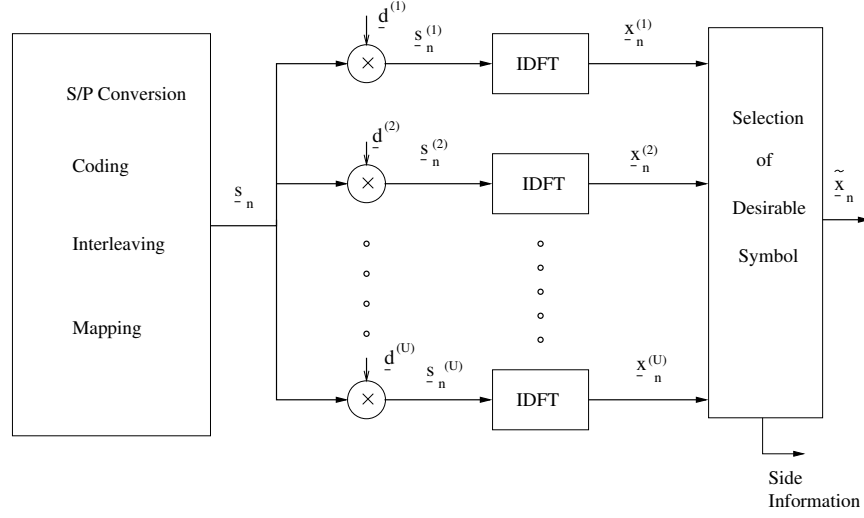
Figure 3.3: Block diagram for SLM-OFDM

A set of U markedly different distinct pseudo-random but fixed vectors $\underline{d}^{(u)} = [d_0^{(u)}, d_1^{(u)}, \ldots, d_{N-1}^{(u)}]$ with $d_v^{(u)} = e^{j\phi_v^{(u)}}$ where $\phi_v^{(u)} \in [0, 2\pi)$, $0 \leq v < N$, $1 \leq u \leq U$ must be defined. The subcarriers vector $\underline{s}_n$ is multiplied subcarrier wise with each of the U vectors $\underline{d}^{(u)}$ resulting in a set of U different subcarrier vectors $\underline{s}_n^{(u)}$ with components

$$s_{n,v}^{(u)} \;=\; s_{n,v} d_v^{(u)} \qquad 0 \leq v < N, 0 \leq u \leq U \tag{3.13}$$

Then all U alternative subcarrier vectors are transformed into time domain to get $\underline{x}_n^{(u)} = IDFT\{\underline{s}_n^{(u)}\}$ and finally the sequence $\underline{\tilde{x}}_n$ with lowest PAPR $\mathcal{X}_n$ is transmitted. Note that one of the alternative subcarrier vectors can be unchanged original one.

The following comments are in order :

➡ Redundancy is introduced to inform the receiver which vector $\underline{d}$ was used for the generation of transmitted OFDM signal in n^{th} block. It is given by $R_{slm} = log_2 U$ bits per OFDM symbol.

➡ Complexity of this scheme is

  – Transmitter : $U\frac{N}{2}log_2 N + (U-1)N$

  – Receiver : $N + \frac{N}{2}log_2 N$

  – Total complexity : $(U+1)\frac{N}{2}log_2 N + UN$

➡ The value of P_w has not reduced but its probability has gone down as CCDF curves have shifted left side as shown in figure 3.4.
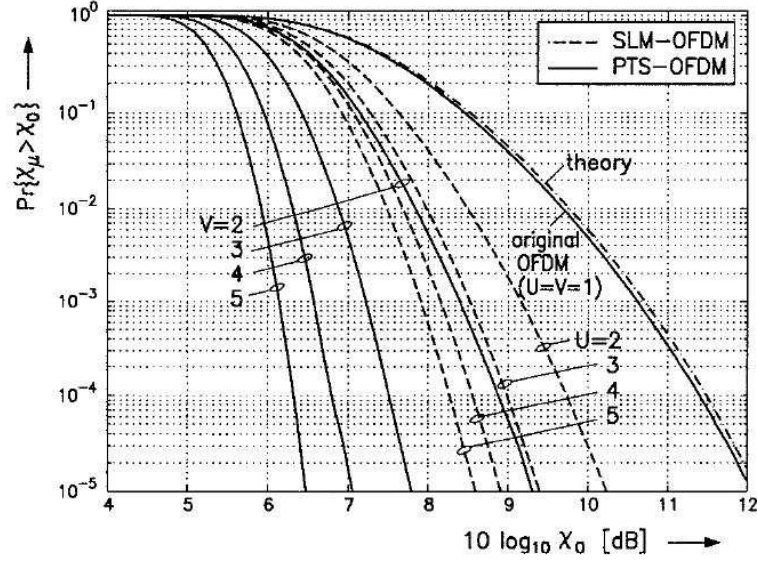
Figure 3.4: CCDF curves (for N=128) for U nos. of IDFT in SLM-OFDM and V nos. of IDFT in PTS-OFDM with W_a=4.

3.4.3   Partial Transmit Sequences

In this scheme [13], [15], the subcarrier vectors $\underline{s}_n$ is partitioned into V pairwise disjoint subblocks $\underline{s}_n^{(v)}$, $1 \leq v \leq V$. All subcarrier positions in $\underline{s}_n^{(v)}$ which are already represented in another subblock are set to zero, so that $\underline{s}_n = \sum_{v=1}^{V} \underline{s}_n^{(v)}$. We introduce complex valued rotation factors $b_n^{(v)} = e^{j\phi_n^{(v)}}$ where $\phi_n^{(v)} \in [0, 2\pi)$, $1 \leq v \leq V$ enabling a modified subcarrier vector

$$\tilde{\underline{s}}_n = \sum_{v=1}^{V} b_n^{(v)} \underline{s}_n^{(v)} \tag{3.14}$$

which represents the same information as $\underline{s}_n$, if the set $\{b_n^{(v)}, 1 \leq v \leq V\}$ (as side information is known for each n). Clearly a joint rotation of all subcarriers in a subblock by the same angle $\phi_n^{(v)} = arg(b_n^{(v)})$ is performed. To calculate $\underline{x}_n = IDFT\{\underline{s}_n^{(v)}\}$, the linearity of IDFT is exploited yielding

$$\underline{x}_n = \sum_{v=1}^{V} b_n^{(v)} IDFT\{\underline{s}_n^{(v)}\} = \sum_{v=1}^{V} b_n^{(v)} \underline{x}_n^{(v)} \tag{3.15}$$

where the V set partial transmit sequences $\underline{x}_n^{(v)} = IDFT\{\underline{s}_n^{(v)}\}$ have been introduced. Based on them a peak value optimization is performed by suitably choosing the free parameters $b_n^{(v)}$. The $b_n^{(v)}$ may be chosen with continuous valued phase angles, but more appropriate in practical systems is a restriction
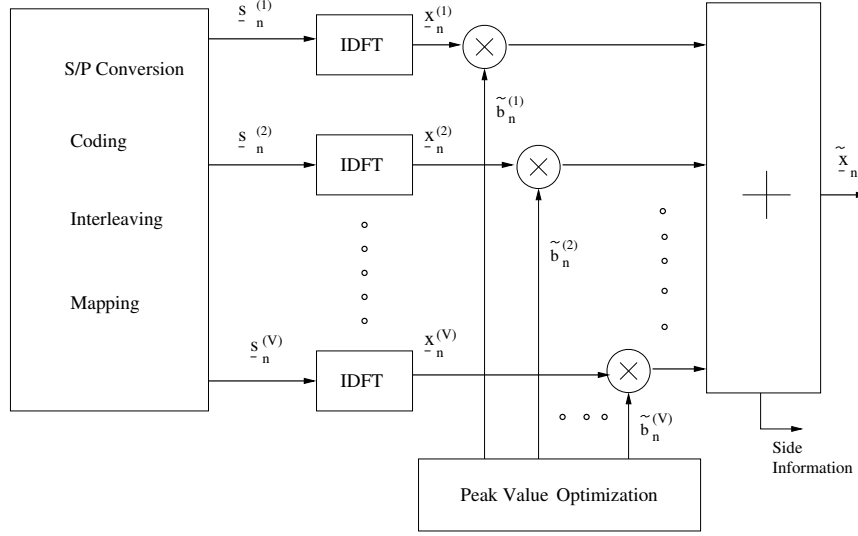
Figure 3.5: Block diagram for PTS-OFDM

on finite set of W_a allowed phase angles. The optimum transmit sequence is then transmitted which is given by

$$\tilde{\underline{x}}_n = \sum_{v=1}^{V} \tilde{b}_n^{(v)} \underline{\tilde{x}}_n \tag{3.16}$$

The PTS-OFDM (Partial Transmit Sequence OFDM) is shown in figure 3.5. Until now, pseudo-random subblock partitioning has found to be best choice for PAPR reduction [13].

Similar to SLM scheme, in this case also P_w (worst case PAPR) is not reduced but its probability does reduce as shown from figure 3.4. Note that PTS can be interpreted as a structurally modified special case of SLM if $W_a^{V-1} = U$ and $\underline{d}^{(u)}$ are chosen in accordance with the partitioning and all the allowed rotation angle combinations $\{b_n^{(v)}\}$. In PTS the choice $b_n^{(v)} \in \{\pm 1, \pm j\}$ ($W_a = 4$) is very interesting for an efficient implementation, as actually no multiplication must be performed, when rotating and combining the PTSs $\underline{x}_n^{(v)}$ to get the peak optimized transmit sequence $\tilde{\underline{x}}_n$.

The following comments are in order

➡ Redundancy of $R_{pts} = (V-1)log_2W_a$ bits per OFDM symbol is needed.

➡ Complexity :

  – Transmitter : $V\frac{N}{2}log_2N + VN$

  – Receiver : $\frac{N}{2}log_2N + N$

  – Total Complexity : $(V+1)(\frac{N}{2}log_2N + N)$

➡ The value of P_w has not reduced but its probability has gone down as CCDF curves have shifted left side as shown in figure 3.4.

3.4.4 Complementary Golay Sequences

Only few data sequences produce signals with high PAPR. With golay codes, we can generate sequences that once modulated with, have PAPR limited to 3dB [2], [21].

A sequence $\underline{x}$ of length N is said to be complementary to another sequence $\underline{y}$ if the following conditions on the sum of autocorrelation function holds

$$\sum_{k=0}^{N-1}(x_k x_{k+i} + y_k y_{k+i}) \quad = \quad 2N \qquad i = 0 \tag{3.17}$$

$$= \quad 0 \qquad i \neq 0 \tag{3.18}$$

There are very interesting relationships between Complementary Golay sequences and Reed Muller code [21], using which, it is easy to design a block algorithm for coding input sequences into Complementary Golay Sequences. These sequences give PAPR of 3dB along with error correction capabilities of Reed Muller codes. Code rate decreases exponentially as N increases. The minimum distance between two different complementary codes of length N is $N/2$ symbols, so it is possible to correct $\frac{N}{4} - 1$ symbol errors or $\frac{N}{2} - 1$ erasures. The Complementary Golay sequences are valid only for phase modulations (PSK) and are not valid for QAM.

Complexity increases exponential with N [2]. For OFDM systems with large number of subcarriers it may not be feasible to generate sufficient number of complementary codes with a length equal to number of channels. To avoid this problem the total number of subchannels can be split into groups of channels at the cost of reduced error correction capability, but this reduces PAPR and increases coderate.

3.4.5 Proposed Scheme : Pulse Shaping for PAPR reduction

It has been seen in earlier section of this chapter, that P_w is caused by the symbol with highest power, when it occurs on all subcarriers in phase. One way to reduce the PAPR is to scale the inputs that modulate the subcarriers differently.

With reference to figure 3.6, consider that all subcarriers are fed symbols $(b_1, b_2 \dots b_N)$ from the same M-PSK constellation. Without loss of generality assume $|b_k| = 1 \ \forall k \in [1, N]$. Here $c_1, c_2, \dots, c_N \geq 0$ are real pulse shaping coefficients (or weights). So we have

$$P_i \quad = \quad \max_t \frac{|x_t|^2}{E[|x_t|^2]} \tag{3.19}$$
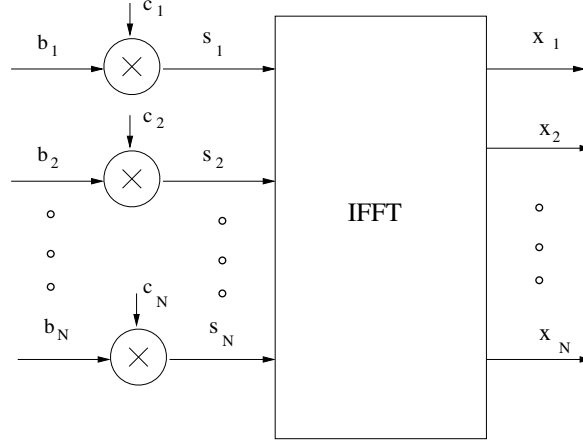
Figure 3.6: Pulse shaping for PAPR reduction

where $x_t = \frac{1}{\sqrt{N}} \sum_{k=1}^{N} s_k e^{j2\pi kt/N}$. Note that $x_t \equiv x(t)$ and $s_k \equiv s(k)$.

$$
\begin{aligned}
E[|x_t|^2] &= E[|s_k|^2] \\
&\approx \frac{|c_1 b_1|^2 + \ldots + |c_N b_N|^2}{N} \\
&= \frac{c_1^2 + \ldots + c_N^2}{N} \\
E[|x_t|^2] &= \frac{1}{N} \sum_{k=1}^{N} c_k^2
\end{aligned}
\tag{3.20}
$$

Now, $\max_t |x_t|^2$ is caused when all the input symbols are in phase i.e.

$$
b_1 = b_2 = \ldots = b_N = b
\tag{3.21}
$$

Therefore, we have

$$
\begin{aligned}
\max_t |x_t|^2 &= \max_t \frac{1}{N} \left| \sum_{k=1}^{N} s_k e^{j2\pi kt/N} \right|^2 \\
&= \max_t \frac{1}{N} \left| b \sum_{k=1}^{N} c_k e^{j2\pi kt/N} \right|^2 \\
&= \frac{1}{N} \left| \sum_{k=1}^{N} c_k \right|^2
\end{aligned}
\tag{3.22}
$$
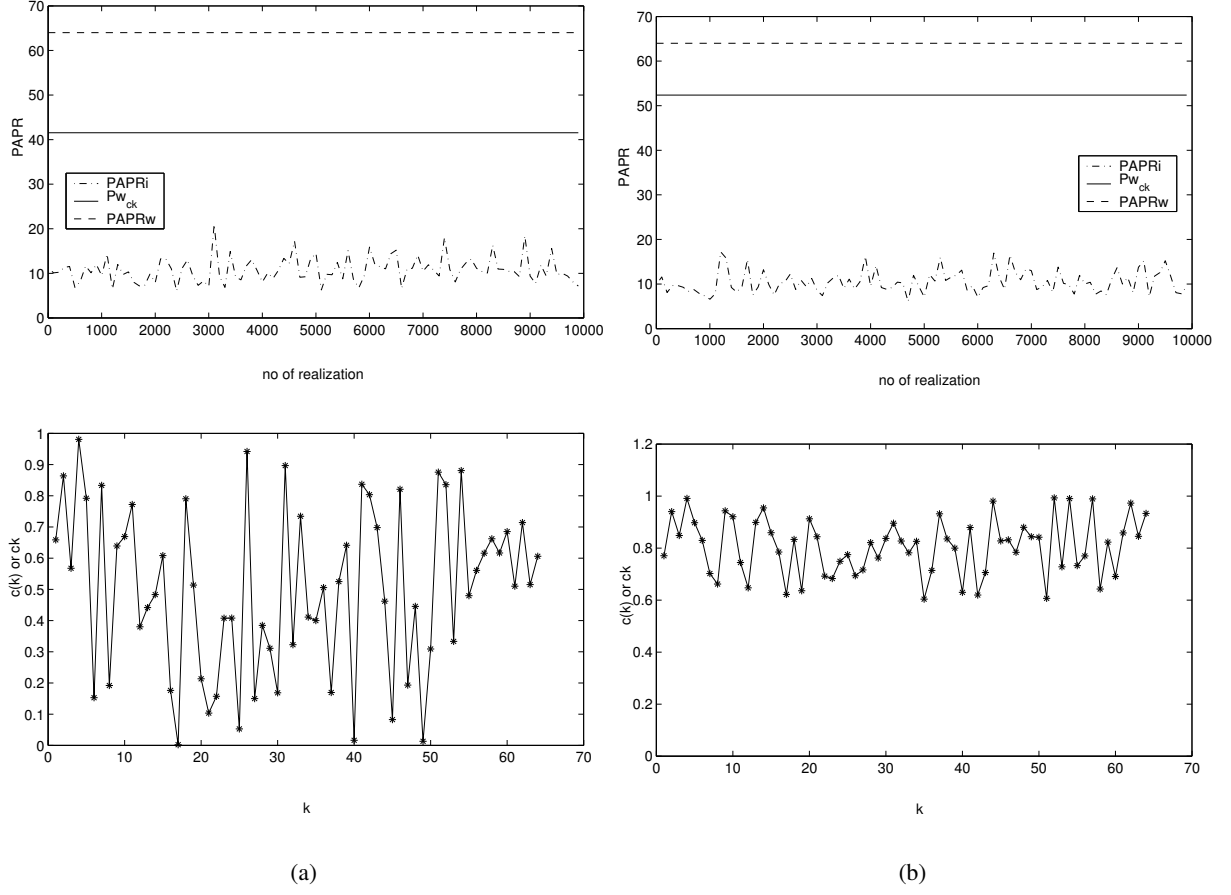
Figure 3.7: Plot of P_i for two 'c' vectors (variation in c_k of fig.(a) is more as compared to fig.(b))

Then upperbound on P_i for given value of c_k's (i.e $\underline{c}$), (denoted as Pw_{ck}) can be written using equations 3.19, 3.20, 3.22, and 3.21 as

$$Pw_{ck} = \frac{\left| \sum c_k \right|^2}{\left| \sum_{k=1}^{N} c_k^2 \right|} \leq N \tag{3.23}$$

Equality holds only if $c_1 = c_2 = \ldots = c_N$.

$$P_i \leq Pw_{ck} \leq P_w \tag{3.24}$$

So it can be seen from above equation that for a given $\underline{c}$, Pw_{ck} serves as new upper bound on P_i that is less than equal to P_w. Thus the upper bound on PAPR is reduced by a factor $G = \frac{N \sum_{k=1}^{N} c_k^2}{(\sum_{k=1}^{N} c_k)^2}$.

Note that even if subcarriers are modulated by symbols from different constellations having dif-

ferent average power, it can be considered to be some constant times one common average power P_{avg} and that constant can be absorbed in c_k. (Similar kind of results have been seen in [17] derived in slightly different way, but we have derived it independently). The optimal power (or bit) loading (water pouring), and channel equalization at the transmitter [1] can be used when CIR is available at the transmitter and it can be seen when these schemes will have unequal c_k's, these schemes reduce PAPR. Reduction in PAPR depends on variation in coefficients c_k's. More the variation, more is the reduction in PAPR as can be seen from figure 3.7. If we are doing channel equalization at the transmitter this will correspond to variation in channel frequency response.

The following comments are in order

➡ Code rate remains unchanged (i.e. same as OFDM without pulse shaping) if we use predetermined <u>c</u>. Otherwise redundancy depends on variation in <u>c</u> (how fast <u>c</u> is changed w.r.t time and how it is conveyed to receiver etc). In case of optimal power (or bit) loading and channel equalization at transmitter, c_k's are dependent on channel. Since channel is known at both receiver and transmitter for this case, redundancy added will be zero.

➡ Complexity of the scheme is given as follows

- Transmitter : $\frac{N}{2}log_2 N + N$
- Receiver : $\frac{N}{2}log_2 N + N$
- Total Complexity : $N log_2 N + 2N$

➡ Upper bound on PAPR is reduced by the factor G.

Chapter 4

SC-FDE and IOFDM

4.1 SC-FDE

4.1.1 Introduction

A single carrier frequency domain equalization (SC-FDE) [18],[19] is a different system itself with similar performance to OFDM, but has low PAPR and hence is discussed here.

An SC-FDE system transmits a single carrier modulated with QAM (or PSK) at high symbol rate. Frequency domain linear equalization in an single carrier system is simply the frequency domain analog of what is done in conventional time domain equalizer. For channels with severe delay spread, FDE is computationally simpler than the corresponding time domain equalization for the same reason OFDM is simpler, because equalization is performed on a block of data at a time and operation on this block involve an efficient FFT operation and a simple channel inversion operation. When combined with FFT processing and the use of a cyclic prefix, SC-FDE has same performance and low complexity as OFDM system.

The SC-FDE system is shown in figure 4.1. Serial to parallel (S/P), parallel to serial (P/S) blocks, RF sections are omitted for convenience.

Noting the similarity between block diagrams for OFDM system and that for SC-FDE, the analysis for OFDM and SC-FDE are quite similar. Hence, we can directly write

$$\underline{z}(n) \;=\; \mathbf{F}_N^H \mathbf{D}^{-1} \mathbf{F}_N \mathbf{R}_{cp} \mathbf{H_0} \mathbf{T_{cp}} \underline{s}(n) + \mathbf{F}_N^H \mathbf{D}^{-1} \mathbf{F}_N \mathbf{R}_{cp} \underline{w}(n) \tag{4.1}$$

Noting that $\mathbf{R}_{cp} \mathbf{H_0} \mathbf{T_{cp}} = \mathbf{F}_N^H \mathbf{D} \mathbf{F}_N$, we have

$$\underline{z}(n) \;=\; \underline{s}(n) + \mathbf{F}_N^H \mathbf{D}^{-1} \mathbf{F}_N \mathbf{R}_{cp} \underline{w}(n) \tag{4.2}$$
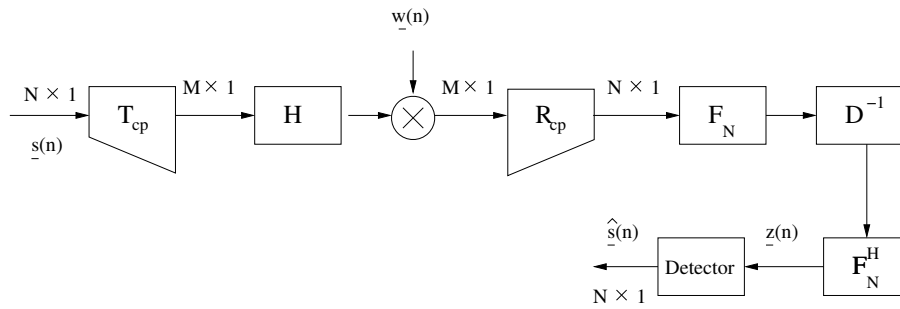
Figure 4.1: Block Diagram for SC-FDE

4.1.2   Comparison between SC-FDE and OFDM

Advantages of SC-FDE as compared to OFDM are [18][19] :

1. Reduced PAPR as no IFFT at the transmitter. Now PAPR is in fact γ_c. This allows the use of less costly power amplifier.

2. Coding while desirable, is not necessary for combating frequency selectivity unlike non-adaptive OFDM.

3. Frequency offset problem is not severe due to absence of multiple carriers.

4. Resistant to narrowband interference.

5. Transmitter complexity is reduced.

Disadvantages of SC-FDE as compared to OFDM [18][19] :

1. Receiver complexity has increased.

2. Optimal bit loading (Water Pouring) cannot be used.

3. Time domain impulsive noise causes error.

There may actually be an advantage in operating a dual mode system, wherein the base station uses an OFDM transmitter and SC-FDE receiver and the subscriber modem uses an SC-FDE transmitter and OFDM receiver as shown in figure 4.2. This arrangement of OFDM in downlink and SC-FDE in uplink has two potential advantages :

1. Concentrating most of the signal processing complexity at the hub or the base station. The hub has two IFFT's and one FFT while the subscriber has only one FFT.

2. The subscriber transmitter is SC-FDE and thus inherently more efficient in terms of power consumption due to reduced power backoff requirements of the SC-FDE mode. This may reduce the cost of a subscriber power amplifier.
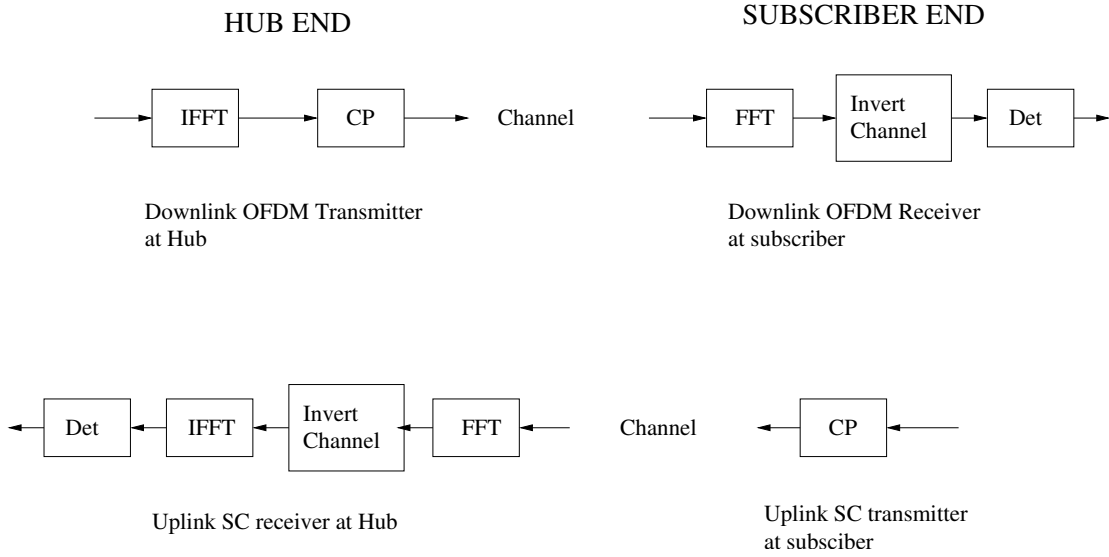
Figure 4.2: Co-existence of SC-FDE and OFDM
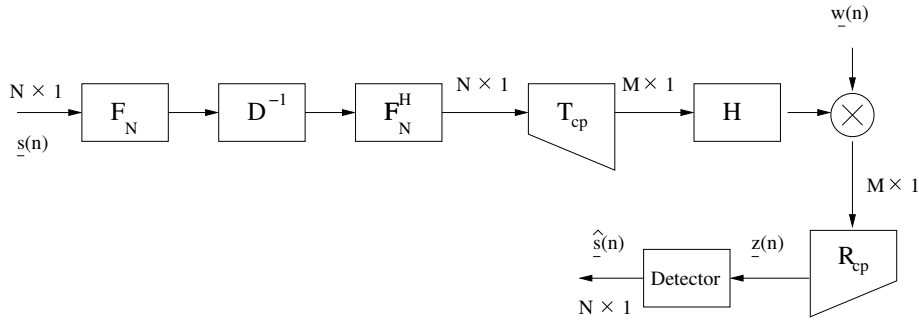
Figure 4.3: SC-FDE Design-II

4.1.3 SC-FDE Design-II

For SC-FDE, design-II as shown in figure 4.3 is proposed here, in which FFT, Equalizer, and IFFT can be shifted to transmitter. Motivation for design II is that if we use the transmitter of original SC-FDE and receiver of design-II at subscriber end and corresponding receiver and transmitter at hub end, then complexity of subscriber will reduce significantly. But the disadvantage of design-II is that PAPR increases considerably and is almost similar to that of OFDM. The simulation results for PAPR of the SC-FDE design-II are shown in figure 4.4.

4.2 IOFDM

In case of OFDM if the channel is constant for a time longer than what it takes to transmit one block of $N + N_g$ symbols, then one is sending more redundant symbols than required i.e. the code rate is
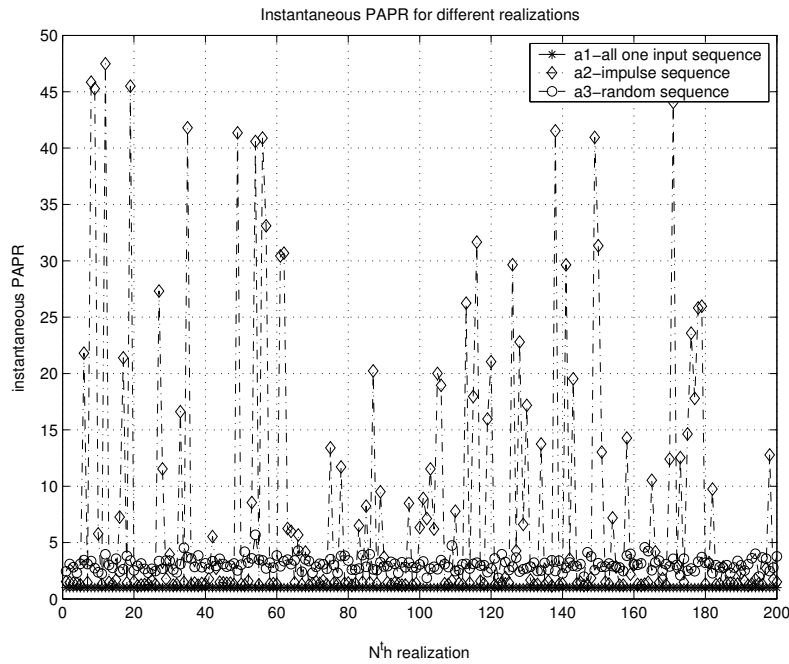
Figure 4.4: PAPR for SC-FDE design-II

reduced. The only way to improve the code rate is to send more symbols per block by increasing number of subcarriers N. The increase in number of subcarriers results in increased PAPR which is undesirable. Interleaved Orthogonal Frequency Division Multiplexing (IOFDM) [5], [6], [7] offers a solution to the problem of improving the code rate without increasing the number of subcarriers and without affecting the PAPR.

We present a second view for IOFDM. We will see IOFDM in light of decreasing PAPR for constant code rate. Figure 4.5 shows transmitter of discrete time baseband model of IOFDM system while figure 4.6 shows its discrete time baseband model of receiver of IOFDM. We denote the number of symbols sent per block as N, but the new number of subcarriers will be denoted by K. In IOFDM N symbols are divided into P blocks of K subcarriers, so that $N = PK$. In original IOFDM, K was kept constant. Therefore with increasing P, N also used to increase. So code rate increases and PAPR is unchanged. From second view, if we keep N constant and vary P, then K decreases. Thus in this case code rate remains unchanged, but PAPR is reduced by factor of P.

We represent a matrix model for IOFDM which is convenient for analysis. Figure 4.7 shows matrix model of IOFDM transmitter. We assume that instead of two blocking stages in figure 4.5, we directly convert the serial data stream $s(n)$ to a parallel data stream $\underline{s}(n)$ with block size of $PK \times 1$. In other words we have

$$\underline{s}(n) = [s(nPK), s(nPK+1), \ldots, s(nPK + PK - 1)] \tag{4.3}$$
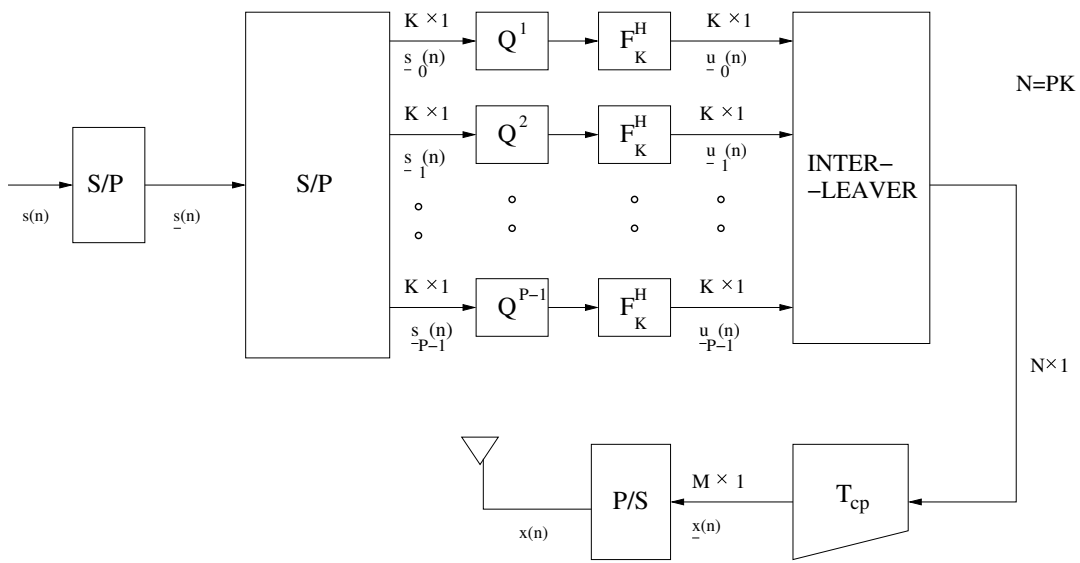
Figure 4.5: IOFDM transmitter
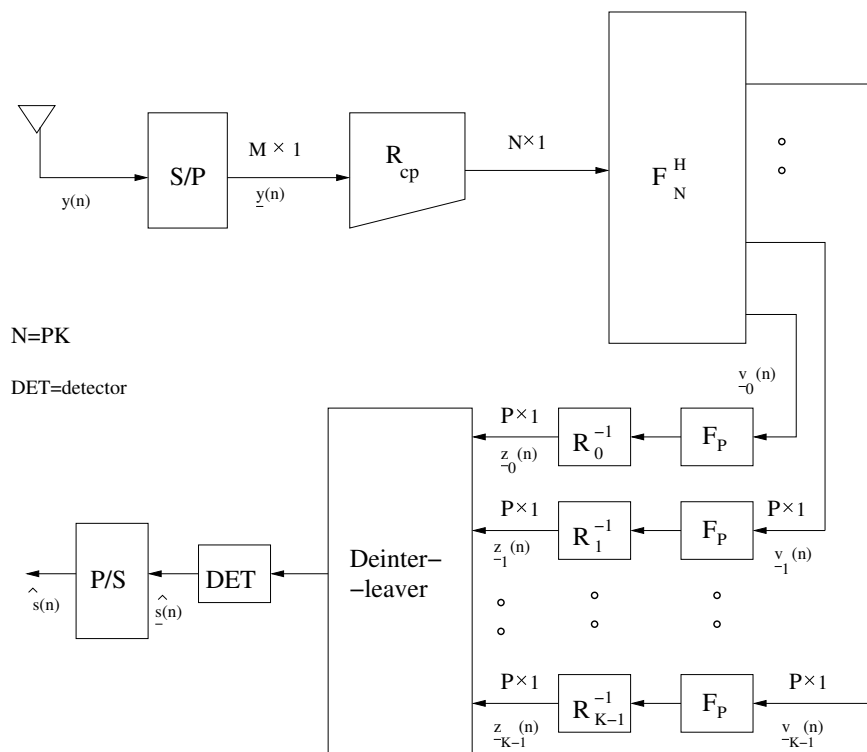
Figure 4.6: IOFDM receiver

N=PK
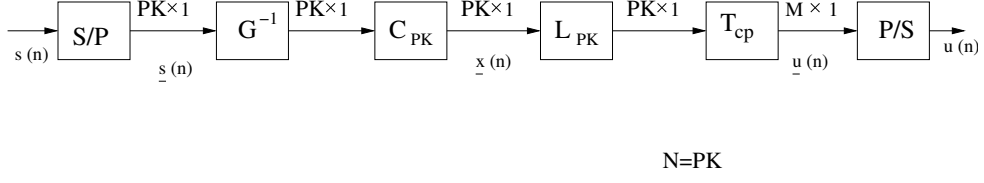
Figure 4.7: Matrix model of IOFDM transmitter

The block stream $\underline{s}(n)$ is then pre-multiplied by $\mathbf{G}^{-1}$ and then precoded by $\mathbf{C_{pk}}$ to give

$$\underline{x}(n) \quad = \quad \mathbf{C_{pk}G}^{-1}\underline{s}(n) \tag{4.4}$$

The precoding matrix has block diagonal structure as follows :

$$\mathbf{C_{pk}} \quad = \quad \begin{bmatrix} \mathbf{F}_K^H & 0 & \ldots & 0 \\ 0 & \mathbf{F}_K^H & \ldots & 0 \\ \vdots & \vdots & \ddots & \vdots \\ 0 & 0 & \ldots & \mathbf{F}_K^H \end{bmatrix} \tag{4.5}$$

and matrix $\mathbf{G}^{-1}$ has the block diagonal form given by

$$\mathbf{G}^{-1} \quad = \quad \begin{bmatrix} \mathbf{Q}^0 & 0 & \ldots & 0 \\ 0 & \mathbf{Q}^1 & \ldots & 0 \\ \vdots & \vdots & \ddots & \vdots \\ 0 & 0 & \ldots & \mathbf{Q}^{P-1} \end{bmatrix} \tag{4.6}$$

where $\mathbf{Q} = diag[1, e^{j2\pi/PK}, e^{j2\pi 2/PK}, \ldots, e^{j2\pi(K-1)/PK}]$. The Precoding matrix $\mathbf{C_{pk}}$ necessarily has a block diagonal structure because it represents P IFFTs of size $K \times K$ that precode each of the P data blocks of $K \times 1$, before they are stacked to obtain the composite $PK \times 1$ data blocks. After precoding, the composite data block is interleaved. The interleaving scheme is shown in figure 4.8. We see that the interleaving consists of placing together every K^{th} symbol from the composite block. This interleaving can be represented as the multiplication of the vector representing the composite $PK \times 1$ block by a permutation matrix. We illustrate this for interleaving of $P = 2$ vectors, each of size 3×1.

$$
\boxed{\text{a1} \;\; \text{a2} \;\; \ldots \;\; \text{ak}} \quad \boxed{\text{b1} \;\; \text{b2} \;\; \ldots \;\; \text{bk}} \quad \boxed{\text{c1} \;\; \text{c2} \;\; \ldots \;\; \text{ck}}
$$

$$\Downarrow \qquad\qquad \Downarrow \text{ Interleaving } \Downarrow \qquad\qquad \Downarrow$$

$$
\boxed{\text{a1} \;\; \text{b1} \;\; \text{c1} \;\; \text{a2} \;\; \text{b2} \;\; \text{c2} \;\; \ldots \;\; \ldots \;\; \text{ak} \;\; \text{bk} \;\; \text{ck}}
$$
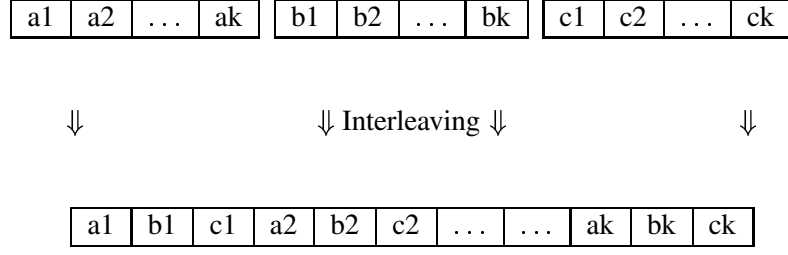
Figure 4.8: Interleaving scheme for IOFDM

$$
\begin{bmatrix}
1 & 0 & 0 & 0 & 0 & 0 \\
0 & 0 & 0 & 1 & 0 & 0 \\
\hline
0 & 1 & 0 & 0 & 0 & 0 \\
0 & 0 & 0 & 0 & 1 & 0 \\
\hline
0 & 0 & 1 & 0 & 0 & 0 \\
0 & 0 & 0 & 0 & 0 & 1
\end{bmatrix}
\begin{bmatrix}
a1 \\ a2 \\ a3 \\ b1 \\ b2 \\ b3
\end{bmatrix}
=
\begin{bmatrix}
a1 \\ b1 \\ a2 \\ b2 \\ a3 \\ b3
\end{bmatrix}
$$

In general the interleaving of P data blocks of size $K \times 1$ to get composite block of size $PK \times 1$ can be represented as the multiplication of a stacked block of P data vectors each of size $K \times 1$, by permutation matrix $\mathbf{L_{pk}}$ [7], which is given by

$$
\mathbf{L_{pk}} \;\; = \;\;
\begin{bmatrix}
\delta_{0,0} & \delta_{1,0} & \ldots & \delta_{P-1,0} \\
\delta_{0,1} & \delta_{1,1} & \ldots & \delta_{P-1,1} \\
\vdots & \vdots & \ddots & \vdots \\
\delta_{0,K-1} & \delta_{1,K-1} & \ldots & \delta_{P-1,K-1}
\end{bmatrix}
\tag{4.7}
$$

where each $\delta_{i,j}$ is $P \times K$ matrix of zeroes, with 1 at the $(i,j)^{th}$ entry. Note that $\mathbf{L}^T \mathbf{L} = \mathbf{L}\mathbf{L}^T = \mathbf{I}$ where $\mathbf{L} = \mathbf{L_{pk}}$. The cyclic prefix is added to interleaved block by cyclic prefix insertion matrix $\mathbf{T_{cp}}$ and are then converted to serial and then transmitted through antenna. Thus the transmitter operation can be represented as

$$
\underline{u}(n) \;\; = \;\; \mathbf{T_{cp}} \mathbf{L_{pk}} \mathbf{C_{pk}} \mathbf{G}^{-1} \underline{s}(n)
\tag{4.8}
$$

The received IBI free vector is given by

$$
\begin{aligned}
\underline{y}(n) &= \mathbf{H_0}\underline{u}(n) + \underline{w}(n) \\
&= \mathbf{H_0}\mathbf{T_{cp}}\mathbf{L_{pk}}\mathbf{C_{pk}}\mathbf{G}^{-1}\underline{s}(n)
\end{aligned}
\tag{4.9}
$$

where the $\mathbf{H}$ is $M \times M$ matrix toeplitz channel convolution matrix. Since the zero pad cancels IBI between the blocks due to channel, we can concentrate on the current blocks alone

$$
\begin{aligned}
\underline{v}(n) &= \mathbf{R}_{cp}\underline{y}(n) \\
&= \mathbf{R}_{cp}\mathbf{H_0}\mathbf{T_{cp}}\mathbf{L_{pk}}\mathbf{C_{pk}}\mathbf{G}^{-1}\underline{s}(n) + \mathbf{R}_{cp}\underline{w}(n)
\end{aligned}
\tag{4.10}
$$

Noting that $\mathbf{R}_{cp}\mathbf{H_0}\mathbf{T_{cp}} = \mathbf{F}_N^H\mathbf{D}\mathbf{F}_N$ from OFDM theory, where $\mathbf{D}$ is diagonal matrix with eigenvalues of $\mathbf{H}$ as diagonal elements. Thus we can rewrite equation 4.10 as

$$
\underline{v}(n) = \mathbf{F}_N^H\mathbf{D}\mathbf{F}_N\mathbf{L_{pk}}\mathbf{C_{pk}}\mathbf{G}^{-1}\underline{s}(n) + \mathbf{R}_{cp}\underline{w}(n)
\tag{4.11}
$$

Taking $\mathbf{F}_N$ and then $\mathbf{D}^{-1}$ we get

$$
\underline{z}(n) = \mathbf{F}_N\mathbf{L_{pk}}\mathbf{C_{pk}}\mathbf{G}^{-1}\underline{s}(n) + \mathbf{D}^{-1}\mathbf{F}_N\mathbf{R}_{cp}\underline{w}(n)
\tag{4.12}
$$

Now we will use the following relationship derived in [7]

$$
\mathbf{F}_N\mathbf{L_{pk}}\mathbf{C_{pk}} = \mathbf{L}^T\mathbf{C}_{\mathbf{kp}}^H\mathbf{L}\mathbf{G}
\tag{4.13}
$$

Noting $\mathbf{L}^T\mathbf{L} = \mathbf{L}\mathbf{L}^T = \mathbf{I}$, and multiplying equation 4.12 by $\mathbf{L}^T(\mathbf{C}_{\mathbf{kp}}^H)^{-1}\mathbf{L}$ we get

$$
\underline{z1}(n) = \underline{s}(n) + \mathbf{L}^T(\mathbf{C}_{\mathbf{kp}}^H)^{-1}\mathbf{L}\,\underline{q}(n)
\tag{4.14}
$$

where $\underline{q}(n) = \mathbf{D}^{-1}\mathbf{F}_N\mathbf{R}_{cp}\underline{w}(n)$. For $\mathbf{L} = \mathbf{L_{pk}}$, $(\mathbf{C}_{\mathbf{kp}}^H)^{-1} = \mathbf{C1_{kp}}$, where $\mathbf{C1_{pk}}$ has block diagonal structure

$$
\mathbf{C1_{kp}} = \begin{bmatrix} \mathbf{F}_P & 0 & \dots & 0 \\ 0 & \mathbf{F}_P & \dots & 0 \\ \vdots & \vdots & \ddots & \vdots \\ 0 & 0 & \dots & \mathbf{F}_P \end{bmatrix}
\tag{4.15}
$$
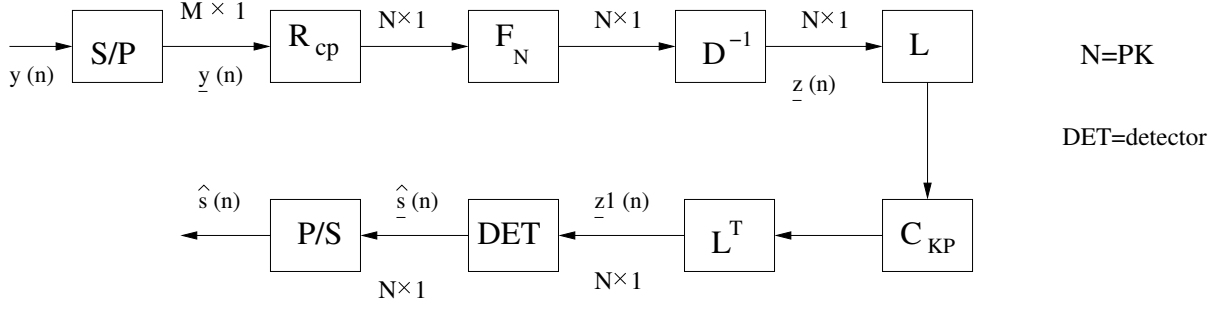
Figure 4.9: Matrix model for IOFDM receiver

That gives the matrix model for the receiver as shown in figures 4.9. It should be noted that from figure 4.6 and 4.9, $\mathbf{LD}^{-1} = diag(\mathbf{R_0^{-1}}, \mathbf{R_1^{-1}}, \ldots, \mathbf{R_{K-1}^{-1}})$, where $\mathbf{R}_l = diag(H(l), H(k+l), \ldots, H((P-1)k+l))$.

The following comments are in order :-

➡ Code Rate : Code rate is $\frac{PK}{PK+N_g}$ i.e $\frac{N}{N+N_g}$ that is same for OFDM with N subcarriers.

➡ PAPR : Since now $K \times K$ IFFT matrices are used at transmitter, P_w is reduced by factor of P. Thus if we go on increasing P, PAPR goes on reducing .

➡ Complexity :

  – Transmitter : $(P-1)K + P(\frac{K}{2}log_2 K)$

  – Receiver : $\frac{N}{2}log_2 N + K(\frac{P}{2}log_2 P)$

  – Total complexity : $(N-K) + N log_2 N$ (slightly more than OFDM).

➡ CCDF curves for IOFDM are similar to OFDM .

4.3 Generalized view of IOFDM

In this section it will be shown that **IOFDM is superset of OFDM and SC-FDE**. Assume noiseless case (without loss of generality) and omit S/P, P/S blocks and antennas for convenience. The OFDM, SC-FDE , and IOFDM systems can be represented by matrix models shown in figure 4.10.

It can be seen that if $P = 1$ (naturally no interleaving) for IOFDM then $\mathbf{L} = \mathbf{L_{pk}} = \mathbf{I}$, $\mathbf{G}^{-1} = \mathbf{I}$, $\mathbf{C_{pk}} = \mathbf{F}_N^H$, and $\mathbf{C_{kp}} = \mathbf{I}$ which results in OFDM. When $P = N$, $K = 1$ (naturally no multiple carriers) then also $\mathbf{L} = \mathbf{L_{pk}} = \mathbf{I}$, $\mathbf{G}^{-1} = \mathbf{I}$, $\mathbf{C_{kp}} = \mathbf{F}_N$, $\mathbf{C_{pk}} = \mathbf{I}$ which results SC-FDE.

OFDM

$\underline{s}(n)$ → F_N^H → T_{cp} → H → R_{cp} → F_N → D^{-1} → $\hat{\underline{s}}(n)$

SC−FDE

$\underline{s}(n)$ → T_{cp} → H → R_{cp} → F_N → D^{-1} → F_N^H → $\hat{\underline{s}}(n)$

$\underline{s}(n)$ → G^{-1} → C_{pk} → L_{pk} → T_{cp} → H → R_{cp}

IOFDM

F_N

$C_{kp} = C1_{kp}$

$\hat{\underline{s}}(n)$ ← L^T ← C_{kp} ← L ← D^{-1}
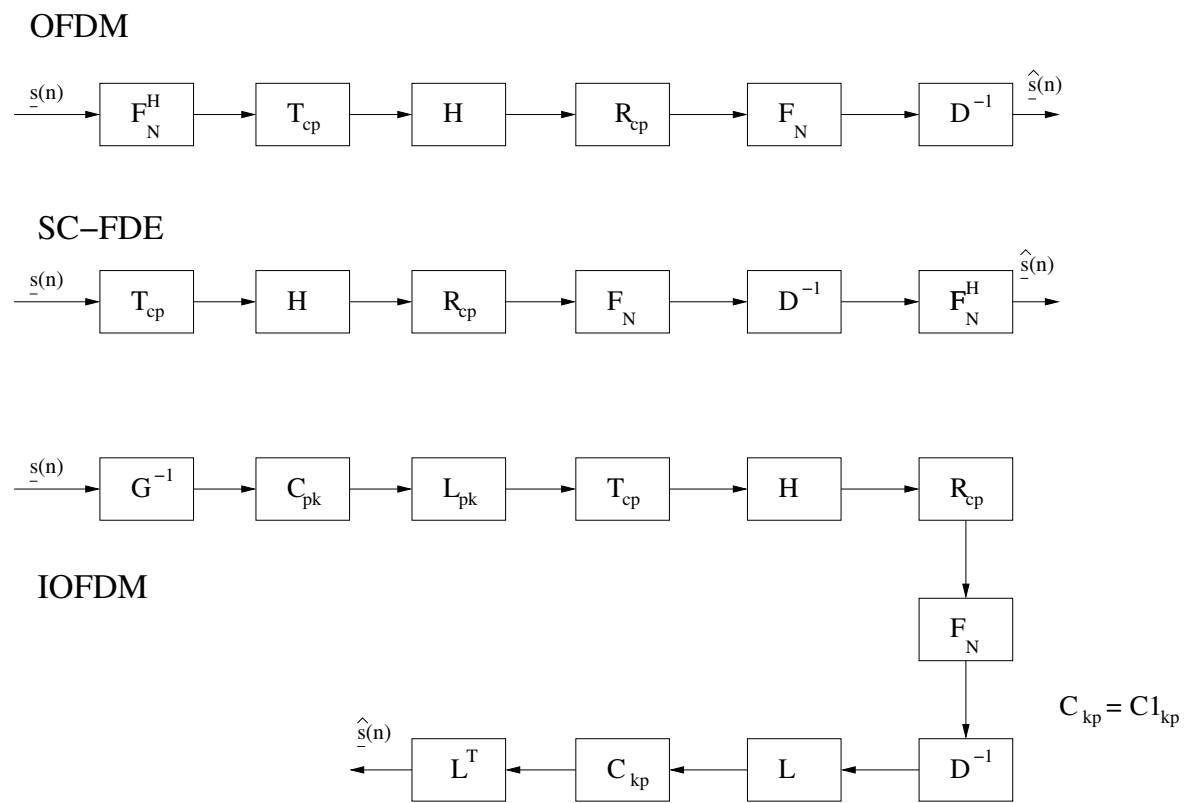
Figure 4.10: Simplified Block Diagrams of OFDM, SC-FDE, and IOFDM systems
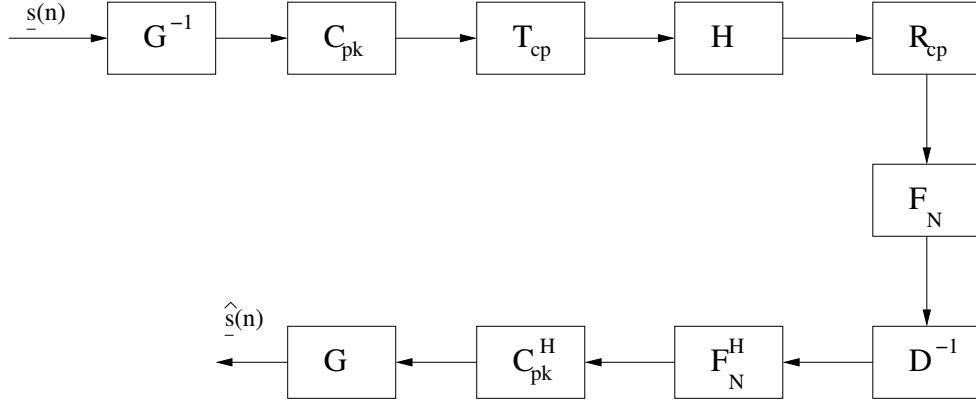
Figure 4.11: Block OFDM

4.4 Block OFDM (BOFDM)

For $1 \leq P \leq N$, IOFDM without interleaving i.e. $\mathbf{L} = \mathbf{L_{pk}} = \mathbf{I}$ (forced no interleaving) from equation 4.13 $\mathbf{C_{kp}}^H \mathbf{G} = \mathbf{F}_N \mathbf{C_{pk}}$ resulting in

$$\mathbf{C_{kp}} \quad = \quad \mathbf{GC_{pk}}^H \mathbf{F}_N^H \tag{4.16}$$

This gives the structure (which we term Block OFDM for reference) is shown in figure 4.11.

It will be shown that **BOFDM is also a Superset of OFDM and SC-FDE.** For $P = 1$, $\mathbf{C_{pk}} = \mathbf{F}_N^H$, which gives OFDM. For $P = N$, $\mathbf{C_{pk}} = \mathbf{I}$ giving SC-FDE.

Note that $\mathbf{G}^{-1}$ at transmitter and $\mathbf{G}$ at the receiver are redundant for BOFDM. Therefore ignoring the $\mathbf{G}$ and $\mathbf{G}^{-1}$ the complexity of BOFDM is

Transmitter : $P(\frac{K}{2}log_2 K) = \frac{N}{2}log_2 K$

Receiver : $Nlog_2 N + P(\frac{K}{2}log_2 K)$

Total complexity : $Nlog_2 N + Nlog_2 K$

Thus the complexity is more as compared to IOFDM. But the difference decreases with decrease in K. In fact, for $K = 1$ BOFDM is slightly less complex than IOFDM as shown in figure 4.12. Thus it can be seen that interleaving has reduced complexity.

4.5 Importance of IOFDM

1. **Trade-off w.r.t subcarriers :** SC-FDE and OFDM are two extremes with respect to number of subcarriers. Each one of the two have some advantages which are disadvantages of the other scheme. So IOFDM can be used to trade off between various parameters to get the best of both schemes (partially). For example, by increasing P (from $P = 1$ i.e. OFDM) PAPR will

reduce, frequency offset problem will reduce, the system will become increasingly resistant to narrowband interference. While increasing P, the problem of time domain impulsive noise will increase and ability to perform water filling decreases.

2. **Comparison of IOFDM, SLM, PTS schemes :** IOFDM reduces the upper bound P_w (with very slight increase in complexity w.r.t. OFDM) by factor of P, as compared to PTS-OFDM and SLM-OFDM where only probability of occurrence of symbols with high PAPR decreases at cost of significant increase in complexity and reduced code rate. Comparison of IOFDM with PTS-OFDM, and SLM-OFDM depends on the P_t (PAPR threshold (in ratio)) chosen (that it is acceptable for the system from the CCDF). For $P_t \geq K$ IOFDM outperforms PTS and SLM schemes in all ways (PAPR reduction, rate, and complexity). For $P_t < K$, IOFDM falls behind only in PAPR reduction with respect to SLM, PTS schemes. Table 4.2 shows comparison of the three schemes (NA=Not Applicable).

-	Redundancy Added w.r.t OFDM			PAPR Reduction (in dB)			Complexity (in no. of multiplications)		
P/U/V	SLM	PTS	IOFDM	SLM	PTS	IOFDM	SLM	PTS	IOFDM
2	1	2	0	2	3	3.01	1600	1344	960
3	1.6	4	0	2.8	4.4	NA	2176	1792	NA
4	2	6	0	3.3	5.2	6.02	2752	2240	992
5	2.3	8	0	3.6	5.8	NA	3328	2688	NA

Table 4.2: Comparison of SLM, PTS, and IOFDM

3. **Motivation for using IOFDM for Golay Sequences :** Golay sequences reduce PAPR to 3dB but rate is reduced drastically while complexity increases with code length. For OFDM systems with large number of subcarriers it may not be feasible to generate sufficient number of complementary codes with a length equal to number of channels. To avoid this problem the total number of subchannels can be split into blocks and IOFDM can be implemented for them. This reduces PAPR and increases coderate at cost of reduced error correction capability.

4. All the schemes discussed in chapter 3 can be readily applied to IOFDM to further reduce the PAPR.
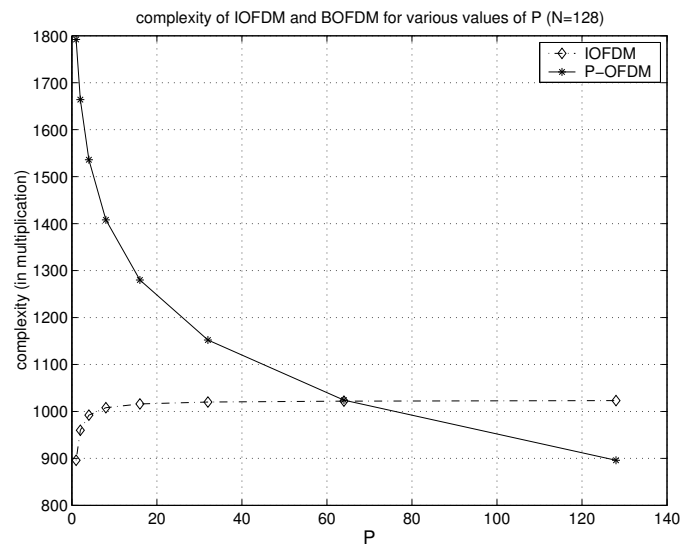
Figure 4.12: Comparison of complexity for IOFDM and BOFDM

Chapter 5

Synchronization

5.1 Introduction

Before an OFDM receiver can demodulate the subcarriers, it has to perform at least two synchronization tasks. First, **Timing Synchronization** i.e. it has to find out the symbol boundaries and the optimal timing instant, to minimize the effects of intercarrier interference (ICI) and intersymbol interference (ISI). Second, **Frequency Offset Correction** i.e. it has to estimate and correct for frequency offset in the received signal, because any offset introduces ICI. In general, Synchronization can be performed with the help of Cyclic Prefix or with special training symbols. In this thesis, we will discuss only special training symbol assisted synchronization.

5.1.1 Sensitivity to Carrier Frequency Offset (CFO)

Sources of Carrier Frequency Offset are the Doppler shift and the differences between local oscillators at the transmitter and the receiver. Such an offset destroys orthogonality between OFDM subcarriers and introduce ICI at the output of the OFDM demodulator. When the frequency offset is larger than the subcarrier spacing F_{sp}, a circular shift of samples at the FFT output can be additionally observed. Thus the total frequency offset can be normalized to the subcarrier spacing and divided into two parts : the integer and fractional ones. Several methods of the estimation of frequency offset can be found in literature [22-27].

If there is frequency offset, the FFT output for each subcarrier will have interfering terms from all subcarriers with an interference power that is inversely proportional to the intercarrier frequency spacing. The degradation in SNR caused by a frequency offset that is small relative to subcarrier spacing [2] is approximated as

$$D_{freq} \approx \frac{10}{3ln10}(\pi \triangle fT)^2 \frac{E_s}{N_o} \tag{5.1}$$

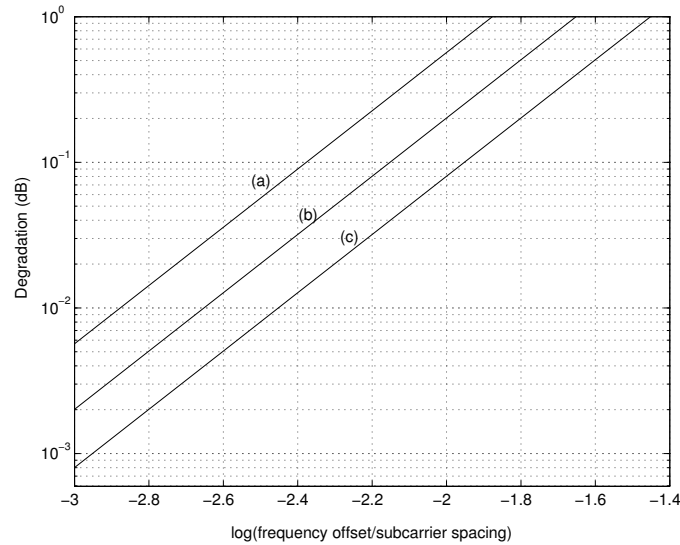The degradation is depicted in figure 5.1 as function of frequency offset per subcarrier spacing and

Figure 5.1: SNR degradation in dB Vs normalized frequency offset for (a) 64 QAM (E_s/N_o=19 dB) (b) 16 QAM (E_s/N_o=14.5 dB) (c) QPSK (E_s/N_o= 10.5 dB)

for 3 different E_s/N_o values. Note for negligible degradation of 0.1 dB, the maximum tolerable frequency offset is less than 1% of the subcarrier spacing. For instance, an OFDM system at a carrier frequency of 5 GHz and a subcarrier spacing of 300kHz, the oscillator accuracy needs to be 3 KHz or 0.6 ppm. The initial frequency error of a low cost oscillator will normally not meet this requirement which means that frequency synchronization has to be applied before FFT.

5.1.2 Sensitivity to Timing Errors

With respect to timing offsets, OFDM is relatively more robust. In fact, the symbol timing offset may vary over an interval equal to the guard time without ICI or ISI, as depicted in figure 5.2. ICI or ISI occurs only when FFT interval extends over a symbol boundary. Hence OFDM demodulation is quite insensitive to timing errors. To achieve the best possible multipath robustness, however, there exists an optimal timing instant, any deviation from which means that the sensitivity to delay spread decreases, so the system can handle less delay spread than the value it was designed for. To minimize this loss of robustness, the system should be designed such that the timing error is small compared with the guard interval.

The timing errors can cause a rotation of the demodulated symbols. The relation between phase ϕ_i of the ith subcarrier and timing offset τ is given by

$$\phi_i \ = \ 2\pi f_i \tau \tag{5.2}$$

where f_i is the frequency of the ith subcarrier before sampling. For an OFDM system with N sub-
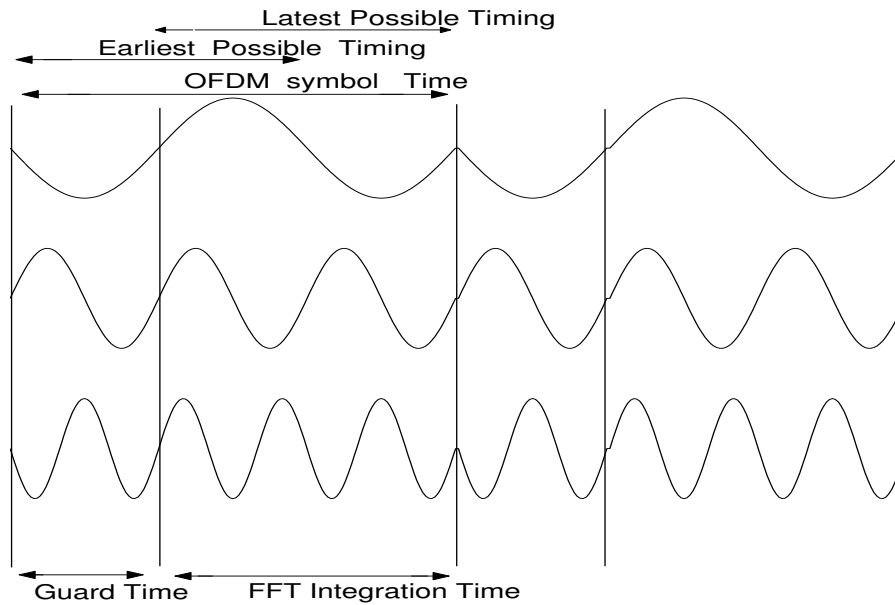
Figure 5.2: Example of OFDM with 3 subcarriers showing the earliest and latest possible timing instants that do not cause ISI or ICI.

carriers and and subcarrier spacing $1/T$, a timing delay of one sampling interval of T/N causes a significant phase shift of $2\pi(1 - 1/N)$ between the first and last subcarrier. Figure 5.3(a) shows an example of the QPSK constellation of a received OFDM signal with 64 subcarriers, an SNR of 30 dB, and a timing offset of 1/16 of the FFT interval. The timing offset translates into a phase offset $2\pi/16$ between the subcarriers. Because of this phase offset, the QPSK constellation points are rotated to 16 possible points on a circle. After estimation and correction of the phase rotation, the constellation diagram of figure 5.3(b) is obtained.

5.2 Synchronization Schemes for OFDM

This section collects various existing algorithm for OFDM. Focus is mainly on synchronization with special training symbols.

5.2.1 Schmidl Cox Algorithm (SCA)

SCA [22] gives a simple method to estimate the symbol synchronization and carrier frequency offset using two training symbols . It can track frequency offset up to many times the subcarrier spacing. Of the two training symbol, the first gives symbol synchronization and the fractional frequency offset (relative to subcarrier spacing) while the second one helps to get the integer part of the frequency offset.

The symbol timing recovery relies on searching for a training symbol with two identical halves

(a) before phase correction

(b) after pahse correction

Figure 5.3: Constellation Diagram with a timing error of $T/16$ before and after phase correction
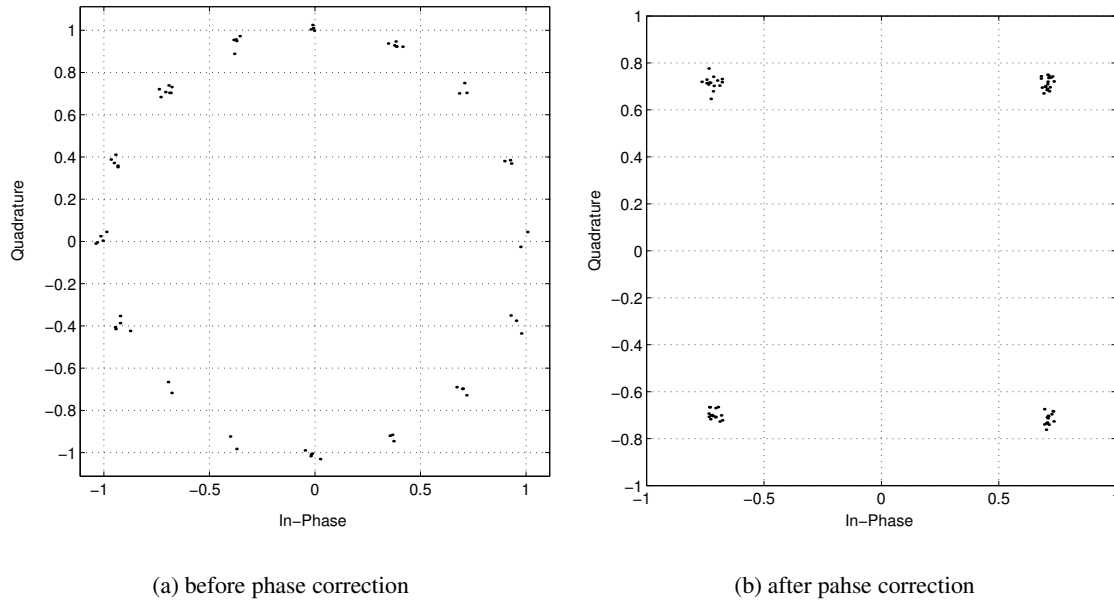
in time domain, which will remain identical after passing through the channel, except that there will be phase difference between them caused by frequency offset. The two halves are made identical (in time order) by transmitting a pseudo noise (PN) sequence on the even subcarrier and zeros along odd subcarriers. The symbol synchronization is obtained by correlating one half of the received block with the next block. The fractional part is obtained by taking the phase of the correlation between the two halves of the data at the optimum sampling point.

The second training symbol contains a PN sequence on odd frequencies to measure these subchannels, and another PN sequence on even subcarriers to help determine integer frequency offset. The ratio of the PN sequence on even subcarriers of second training symbol to PN sequence on even subcarriers of first training symbol is denoted by v. This, along with PN sequences on even subcarriers of both training symbols, is used to obtain the integer part of the frequency offset.

5.2.1.1 Symbol Synchronization

Consider the first training symbol where the first half is identical to the second half (in time order), except for a phase shift caused by the carrier frequency offset. If the conjugate of the sample from the first half is multiplied by the the corresponding sample from second half ($T/2$ seconds later), the effect of channel should cancel, and the result will have a phase approximately of $\phi = \pi T \triangle f$. At the start of frame, the product of each of these will have approximately same phase, so the magnitude of the sum will be large value.

Let $r_m = y_m + \eta_m$ be the received vector where y_m is x_m convolved with channel (but without
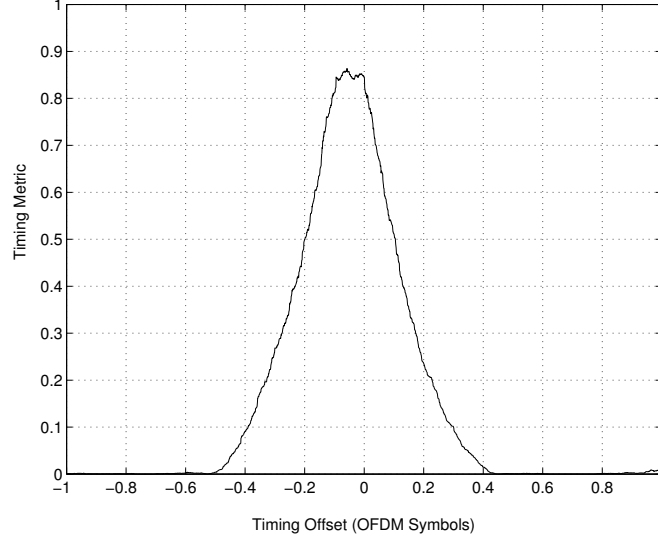
Figure 5.4: Example of Timing Metric for AWGN channel (SNR=10 dB, N=1024)

noise). Let there be ℓ complex samples in one half of the first training symbol (excluding cyclic prefix), and let the sum of the pairs of the products be

$$P(d) \quad = \quad \sum_{m=0}^{\ell-1} r^*_{d+m} r_{d+m+\ell} \tag{5.3}$$

which can be implemented with the iterative formula

$$P(d+1) \quad = \quad P(d) + (r^*_{d+\ell} r_{d+2\ell}) - (r^*_d r_{d+\ell}) \tag{5.4}$$

Note that d is a time index corresponding to the first sample in a window of 2ℓ samples. This window slides along in time as the receiver searches for the first training symbol. The received energy for the second half-symbol is defined by

$$R(d) \quad = \quad \sum_{m=0}^{\ell-1} |r_{d+m+\ell}|^2 \tag{5.5}$$

A Timing metric can be defined as

$$M(d) \quad = \quad \frac{|P(d)|^2}{(R(d))^2} \tag{5.6}$$

Figure 5.4 shows an example of timing metric as a window slides past coincidence for the AWGN channel for an OFDM signal with 1024 subcarriers, a CFO of 12.4 subcarrier spacing and SNR=10 dB where SNR is total signal power (all subcarriers) to noise power ratio. Guard interval is taken to be 10% of the useful part (=102 samples). The timing metric reaches a **plateau** which has **length of the guard interval minus the length of channel impulse response** since there is no ISI within the plateau to distort the signal. For the AWGN channel, there is window with a length of the guard interval where the metric reaches a maximum, and the start of frame can be taken anywhere within the window without a loss in the received SNR. For the frequency selective channels, the length of impulse response of the channel is shorter than the guard interval by design choice of the guard interval, so the plateau in the maximum of the timing metric is shorter than for AWGN channel. This plateau leads to some uncertainty as to start of the frame. To avoid this uncertainty it uses second method in which a maximum is found, then the points to the left and right are located in the time domain, which are 90% of maximum and this two points (90%), are averaged to find the symbol timing estimate.

Performance of Symbol Timing Estimator : -

Distribution of metric at the optimum timing [22] is given by

$$M(d_{opt}) \quad \sim \quad \mathcal{N}(\mu_M, \sigma_M^2)$$

where

$$\mu_M \quad = \quad E[M(d_{opt})] = \frac{\sigma_s^4}{(\sigma_s^2 + \sigma_n^2)^2} \quad , \tag{5.7}$$

$$\sigma_M^2 \quad = \quad var[M(d_{opt})] = \frac{2\sigma_s^4[(1 + \mu_M)\sigma_s^2\sigma_n^2 + (1 + 2\mu_M)\sigma_n^4]}{\ell(\sigma_s^2 + \sigma_n^2)^4} \quad . \tag{5.8}$$

For high SNR, $\mu_M \approx 1$ and $\sigma_M^2 = \frac{4}{\ell \cdot SNR}$, where $E[Re\{y_m^2\}] = E[Im\{y_m^2\}] = \sigma_s^2$, $E[Re\{\eta_m^2\}] = E[Im\{\eta_m^2\}] = \sigma_n^2$, and $SNR = \frac{\sigma_s^2}{\sigma_n^2}$.

The distribution of metric outside the first symbol is given by

$$M(d_{outside}) \quad \approx \quad \frac{1}{\ell} \mathcal{X}_2^2 \tag{5.9}$$

where $\mathcal{X}_2^2$ is central chi square pdf with two degrees of freedom with mean 2 and variance 4. Therefore mean and variance for metric outside the first symbol are given by

$$E[M(d_{outside})] \quad = \quad \frac{1}{\ell} \tag{5.10}$$

(a) At correct timing instant   (b) At incorrect timing instant
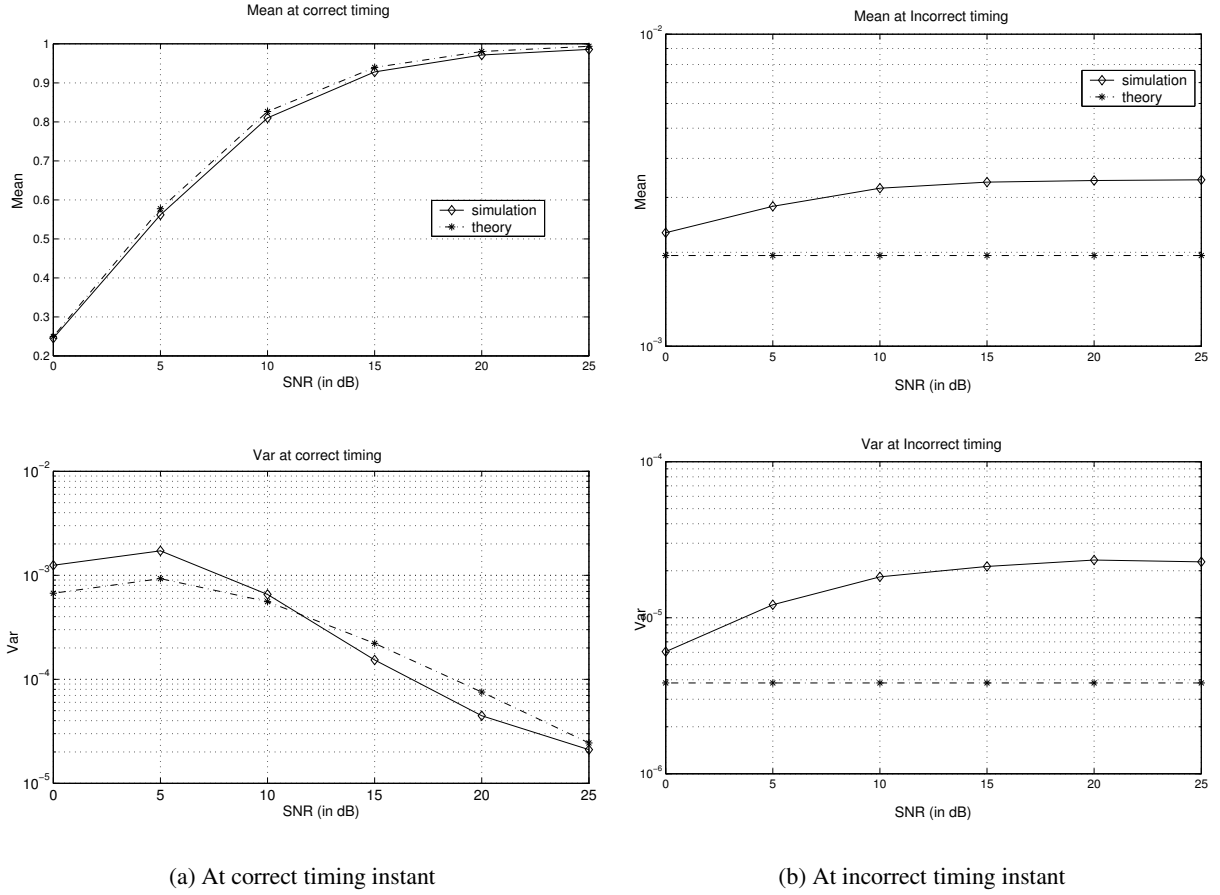
Figure 5.5: Mean and variance at correct and incorrect timing instant for ISI channel

$$var[M(d_{outside})] = \frac{1}{\ell^2} \tag{5.11}$$

Figure 5.5 shows the simulated and theoretical curves for mean and variance of the metric at an optimum sampling point and outside for an exponential Rayleigh channel . For each SNR value, the simulation was run 10,000 times, each time generating different PN sequences, channel realization, and noise.

5.2.1.2 Carrier Frequency Offset (CFO) Estimation

The two halves of the first training symbol have a phase difference of $\phi = \pi T \triangle f$ in absence of noise, where T is time duration of the OFDM Symbol (without CP) and $\triangle f$ is frequency offset. Under noise, an estimate of this can be obtained as

$$\hat{\phi} = \angle P(d) \tag{5.12}$$

The fractional part of the frequency offset relative to the subcarrier spacing ϵ_{frac} can now be obtained as

$$\epsilon_{frac} = \frac{\hat{\phi}}{\pi} \tag{5.13}$$

The actual frequency offset is $\frac{\phi}{\pi T} + \frac{2z}{T}$ where z is some integer. By partially correcting the frequency offset, adjacent carrier interference (ACI) can be avoided, and then the remaining offset $2z/T$ can be found. After the two training symbols are frequency corrected by $\hat{\phi}/(\pi T)$, let their FFT's be $Y_{1,k}$ and $Y_{2,k}$, where $Y_{i,j}$ corresponds to the retrieved data for i^{th} symbol and j^{th} subcarrier. An integer shift in relative frequency will be reflected as a shift in data. Define $\mathcal{Y}$ as the set of indices for the even frequency components, $\mathcal{Y}=\{-W, -W+2, \ldots, -4, -2, 2, 4, \ldots, W, W-2, W\}$ where $W = N/2$. The number of even positions shifted can be calculated by finding $\hat{g}$ to maximize

$$B(g) = \frac{\left| \sum_{k\epsilon\mathcal{Y}} Y^*_{1,k+2g} v^*_k Y_{2,k+2g} \right|^2}{2(\sum_{k\epsilon\mathcal{Y}} |Y_{2,k}|^2)^2} \tag{5.14}$$

where $v_k = \frac{\sqrt{2}\, s_{2,k}}{s_{1,k}}$ with $s_{i,j}$ corresponding to the actual data on j^{th} subcarrier of ith training symbol. The frequency offset estimate then becomes

$$\widehat{\triangle f} = \frac{\hat{\phi}}{\pi T} + \frac{2\hat{g}}{T} \tag{5.15}$$

Variance of fractional estimate [24][28], for usable SNR values and sufficiently large value of ℓ, is given by

$$var[\frac{\hat{\phi}}{\pi}] \geq \frac{1}{\pi^2 \ell\, SNR} \tag{5.16}$$

This is indeed CRLB (Cramer Rao Lower Bound) which is not very surprising as the method for fractional frequency offset estimation is an ML estimate [24]. Now if the integer part estimation is correct, the total variance will be just that of fractional part.

The distribution for the metric $B(g)$ is Gaussian [22] with mean and variance given by

$$E[B(g_{correct})] = \frac{\sigma_s^4}{(\sigma_s^2 + \sigma_n^2)^2} = \frac{SNR^2}{(SNR+1)^2} \tag{5.17}$$

$$var[B(g_{correct})] = \frac{\sigma_s^4[(1+2\mu_B)\sigma_s^2\sigma_n^2 + (1+4\mu_B)\sigma_n^4]}{W(\sigma_s^2 + \sigma_n^2)^4} \tag{5.18}$$
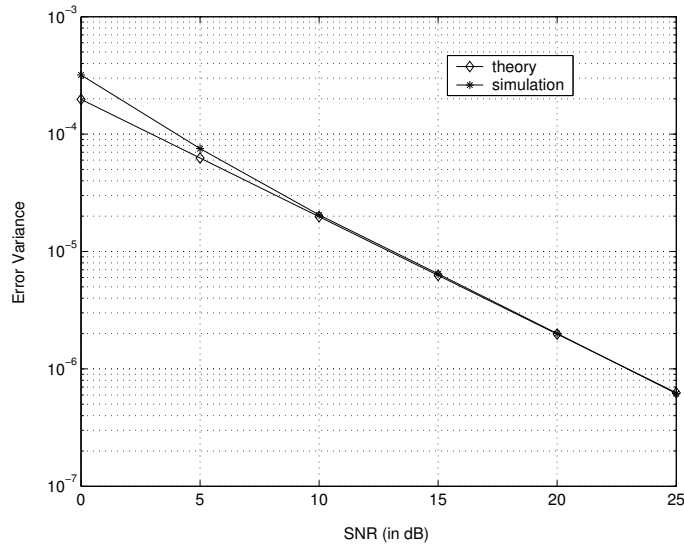
Figure 5.6: Performance of frequency offset estimator (fractional + integer part) for an exponential Rayleigh channel with N=1024

While at incorrect frequency offset, $B(g)$ has chi-square distribution with 2 degrees of freedom and mean and variance given by

$$E[B(g_{incorrect})] \quad < \quad \frac{1}{W} \tag{5.19}$$

$$var[B(g_{correct})] \quad < \quad \frac{1}{W^2} \tag{5.20}$$

Finally performance of joint frequency offset estimator is shown in figure 5.6 for N=1024, exponential Rayleigh channel and frequency offset 2.4 subcarrier spacing. For each SNR value, the simulation was run 10,000 times, each time generating different PN sequences, channel realizations, and noise.

5.2.2 Minn Zeng Bhargava (MZB) Algorithm

In SCA, the timing metric reaches a plateau which leads to some uncertainty as to where the start of frame is. This causes large variance of timing estimate. To improve on this, following methods were proposed in [23].

5.2.2.1 Sliding Window Method (Method A)

In calculation of the half-symbol energy $R(d)$, all samples over one symbol period is used instead of the second half symbol period. Next, instead of 90% points averaging, the timing metric is simply

averaged over a window of length of $N_g + 1$ samples where N_g is length of cyclic prefix. Then the timing metric is given by

$$M_1(d) \quad = \quad \frac{1}{N_g + 1} \sum_{k=-Ng}^{0} M_f(d + k) \tag{5.21}$$

where $M_f(d)$ can be calculated as

$$M_f(d) \quad = \quad \frac{|P(d)|^2}{R_f^2(d)} \tag{5.22}$$

$$R_f(d) \quad = \quad \frac{1}{2} \sum_{m=0}^{N-1} |r(d + m)|^2 \tag{5.23}$$

and $P(d)$ is given by equation 5.3. The symbol timing estimate is taken as the argument of maximum of this metric, $M_1(d)$.

5.2.2.2 Training Symbol Method (Method B)

The samples of training symbol method (excluding CP) are designed to be of the form

$$S \quad = \quad [A \ A \ - A \ - A] \tag{5.24}$$

where A represents samples of length $\ell_1 = N/4$ generated by $N/4$ point IFFT and data modulated by PN sequence such that sum of the corresponding data equals zero. Then the timing metric is given by

$$M_2(d) \quad = \quad \frac{|P_2(d)|^2}{R_2^2(d)} \tag{5.25}$$

where

$$P_2(d) \quad = \quad \sum_{k=0}^{1} \sum_{m=0}^{\ell_1 - 1} r^*(d + 2k\ell_1 + m) \cdot r(d + 2k\ell_1 + m + \ell_1) \tag{5.26}$$

$$R_2(d) \quad = \quad \sum_{k=0}^{1} \sum_{m=0}^{\ell_1 - 1} |r(d + 2k\ell_1 + m + \ell_1)|^2 \tag{5.27}$$

In both methods $P_2(d)$ and $R_2(d)$, or $P(d)$ and $R_f(d)$ can be calculated iteratively as in case of SCA. The timing metric of SCA and MZB are shown in figure 5.7 under no noise and distortion
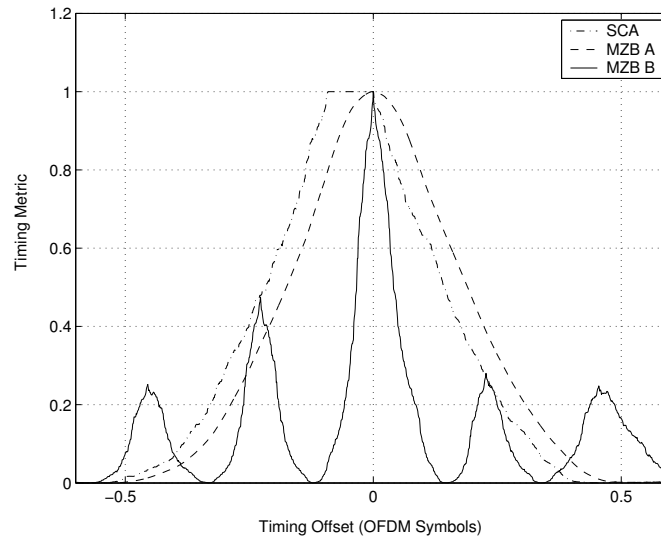
Figure 5.7: Timing Metric of SCA and MZB under no noise and distortion condition

condition with the system parameter $N = 1024$, $N_g = 102$.

5.2.2.3 Simulations and Discussion

Performance of timing offset estimators have been investigated for following five cases : -

1. SCA with 90% Averaging

2. SCA (as in 1) with $R(d)$ replaced by $R_f(d)$.

3. Method A

4. Method B

5. Method B with $R_2(d)$ replaced with $R_f(d)$

The system used 1024 subcarriers OFDM system with 1024 point FFT, 10% guard interval (102 samples), CFO of 12.4 subcarrier spacing, BPSK modulation. For each SNR value, the simulation was run 10,000 times, each time generating different PN sequences, channels, and noise. Two channel were considered (i)AWGN and (ii) ISI (Exponential Rayleigh) with channel order=16.

Figure 5.8 and 5.9 show the mean and variance of the timing offset in AWGN channel and ISI channel resp. For AWGN, means of cases 1 and 2 are in middle of plateau while for other cases it is about correct timing point. For ISI, they are slightly shifted to the right in time axis by some amount depending on shape of timing metric and ISI channel. Note that if the timing estimate is desired to be within guard interval, then the means of 3-5 cases can be shifted to left (in advanced) by appropriate design amount.
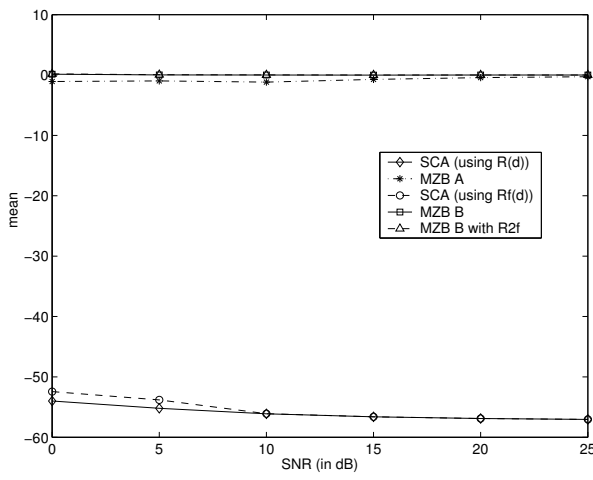
(a) Mean vs SNR
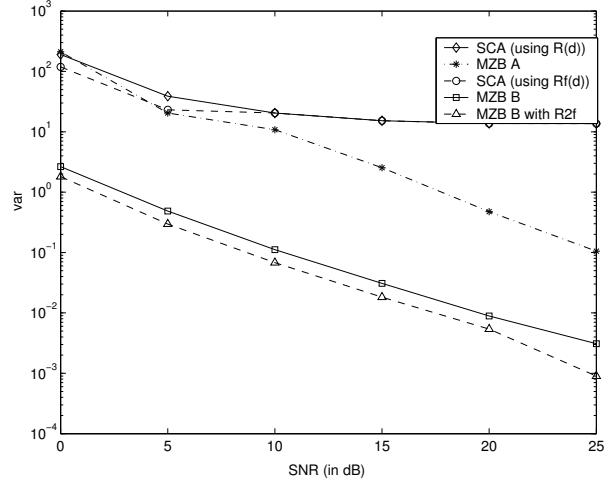
(b) Variance vs SNR

Figure 5.8: mean and variance of SCA and MZB in AWGN
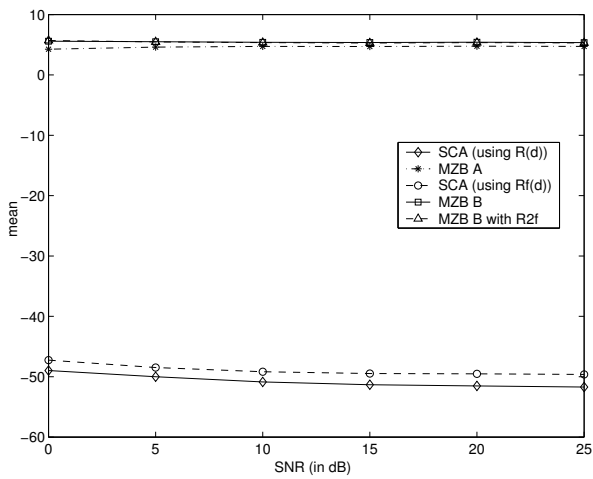
(a) Mean vs SNR
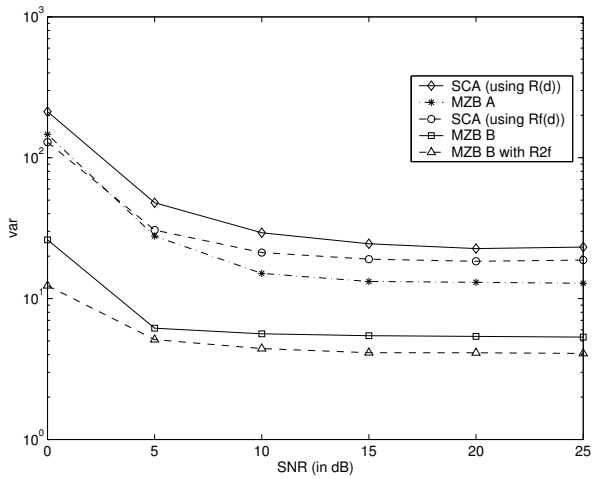
(b) Variance vs SNR

Figure 5.9: mean and variance of SCA and MZB in ISI

MZB method has significantly less variance than SCA because of absence of plateau in timing metric. In AWGN channel, cases 1-2 show floor variance, but 3-5 do not. In ISI channel, all of them have floor variance. Using $R_f(d)$ instead of $R(d)$ gives better performance. Overall 'case 5' has best performance.

Chapter 6

Proposed Scheme : Tone based IFO estimation

This scheme is based on the fact that Integer Frequency offset (IFO) causes data to be cyclically shifted. Noting this simple fact, if we send pure tone i.e. data on only one subcarrier of the training symbol and detect the shift in the position of this impulse (in frequency domain), the required IFO can be obtained.

At transmitter, the data modulating the subcarriers for IFO training symbol is

$$s(k) = \begin{cases} \sqrt{NP_s} & k = k_0 \\ 0 & k \neq k_0 \end{cases} \tag{6.1}$$

$\sqrt{NP_s}$ is required because of constraint that the average power per OFDM symbol is the same. Let $x(t)$=IFFT$\{s(k)\}$, where $k, t\epsilon[0, N-1]$. Note $x(t)$ are transmitted symbols. Let $x(t_c)$ be the corresponding continuous time signal and $y(t_c)$ be the received (continuous) signal (without noise and channel distortion) after frequency offset of $\triangle f$ at receiver, then

$$y(t_c) = x(t_c)e^{j2\pi\triangle f t_c}$$

and in discrete time domain the same equation can be written as

$$y(t) = x(t)e^{j2\pi t\triangle k/N}$$

where $\triangle k = \frac{\triangle f}{F_{sp}}$, is frequency offset (FO) normalized to subcarrier spacing F_{sp}. Taking FFT, we get

$$Y(k) = s(k - \triangle k) \quad \forall k \tag{6.2}$$

So from equations 6.1 and 6.2, we have

$$Y(k) = \begin{cases} \sqrt{NP_s} & k = k_0 + \triangle k \\ 0 & k \neq k_0 \end{cases} \tag{6.3}$$

Thus argument corresponding to maximum of $Y(k)$ will have sufficient information about frequency offset. If size of FFT at the receiver is sufficiently large, then both the fractional part and the integer part can be estimated jointly. Unfortunately, this will result in high computational complexity.

The timing synchronization and fractional frequency offset correction have to be necessarily performed before IFO. Hence the same is assumed here. In fact, we show later that SCA can be used in conjunction with IFO training symbol for timing synchronization and fractional frequency offset correction. So we will concentrate on IFO estimation only. Assuming that fractional part of frequency offset has been removed, we can estimate the integer frequency offset as follows

$$C(k) = |Y(k)|^2 \tag{6.4}$$

$$k_0' = arg\{\max_k C(k)\} \tag{6.5}$$

$$\widehat{\triangle k_i} = k_0' - k_0 \tag{6.6}$$

where $\widehat{\triangle k_i}$ will be integer such that $-k_0 \leq \widehat{\triangle k_i} < N - k_0$.

6.1 Some Observations for Proposed Scheme

1. Fractional frequency part by SCA gives an estimate in range of ± 1 subcarriers. Therefore if we are sending impulse on an even subcarrier, then **only even subcarriers need to be searched**.

2. **Frequency Acquisition range,** the range of integer frequency offsets that can be corrected, is $(N - k_0) - k_0 = N$ subcarriers i.e. entire OFDM bandwidth.

3. To change the frequency acquisition span from $-k_0 \leq \triangle k_i < N - k$ to $-k_0 + g \leq \triangle k_i < N - k + g$, construct new search vector $C_1(k) = C(k - g)$, i.e. $\underline{C}_1 = [C(g), C(g+2), \ldots C(N-2), C(0) \ldots C(g-2)]$. Thus for $\triangle k_i$ to be in range $[-N/2, N/2]$, $g = k_0 + N/2$. Note that $\triangle k_i$, k and g are all even when impulse is sent on even subcarrier.

4. It is evident from equation 6.6, that the scheme is **independent of subcarrier** on which an impulse is sent.

5. **Scheme is independent of timing errors if starting of frame is in plateau of length (CP-L).** This is straight forward, noting that timing offset will cause phase rotation in frequency domain and our metric (see equation 6.5) is independent of phase rotation.

6. The **similarity between the proposed scheme and M-orthogonal signaling** (specially FSK) scheme should be noted where one transmits 1 out of M orthogonal signals. In that case the optimal detector is given by equations 6.4 and 6.5. In fact, this scheme is M-orthogonal signaling used for IFO estimation with slight modification.

7. For timing synchronization and fractional frequency offset correction in SCA, two identical halves in time domain are required. When impulse is sent on an even subcarrier, we get two identical halves in time domain of one OFDM symbol, so that SCA algorithm can be used for timing synchronization and fractional frequency offset estimation in conjunction with IFO training symbol. So our **earlier assumption that fractional frequency offset is already corrected for proposed scheme is valid**.

8. If impulse is sent on any of the odd frequencies then we get two out of phase halves in one OFDM symbol which can be used for SCA with phase modification (multiplication by -1 to latter half) and rest of discussion will be similar to the one for even frequency.

9. Total frequency offset can be given as in equation 5.15,

$$\widehat{\triangle f} \quad = \quad \frac{\hat{\phi}}{\pi T} + \frac{2\widehat{\triangle k_i}}{T} \tag{6.7}$$

6.2 Mathematical Analysis

6.2.1 Data Model 1 : AWGN Channel

Data modulating the subcarriers of the training symbol are

$$s(k) \quad = \quad \begin{cases} \sqrt{NP_s} & k = k_0 \\ 0 & k \neq k_0 \end{cases} \tag{6.8}$$

Note that $0 \leq k \leq N - 1$ and $0 \leq t < N$ throughout the analysis unless specified otherwise. After IFFT stage at the transmitter, we have

$$x(t) \quad = \quad \frac{1}{\sqrt{N}} s(k_0) e^{j2\pi k_0 t/N} \quad \forall t = 0, \ldots, N - 1 \tag{6.9}$$

Let $w(t)$ be AWGN noise with i.i.d real and imaginary part, each having variance σ_n^2 i.e

$$w(t) \quad \sim \quad \mathcal{N}(0, \sigma_n^2) + j\mathcal{N}(0, \sigma_n^2) \tag{6.10}$$

Hence signal power = $\frac{1}{N} \sum_{n=0}^{N-1} |x(t)|^2 = P_s$, and Noise Power = $2\sigma_n^2$. Therefore

$$SNR \quad = \quad \frac{P_s}{2\sigma_n^2} \tag{6.11}$$

The received signal is

$$z(t) \quad = \quad x(t) + w(t) \tag{6.12}$$

After frequency offset (without loss of generality assume FO to be integer only), the received signal is

$$y(t) \quad = \quad z(t)e^{j2\pi t \triangle k_i / N} \tag{6.13}$$

Taking FFT of both sides, we get

$$Y(k) \quad = \quad s(k - \triangle k_i) + W(k - \triangle k_i) \quad k = k_0' \tag{6.14}$$

where $W(k)$ is FFT of $w(t)$. Noting that $k_0 = k_0' - \triangle k_i$, we get

$$Y(k) \quad = \quad \begin{cases} s(k_0) + W(k_0) & k = k_0' \\ W_1(k) & k \neq k_0' \end{cases} \tag{6.15}$$

where $W_1(k) \triangleq W(k - \triangle k_i)$. Since $w(t)$ are i.i.d Gaussian random variables, $W(k)$ and $W_1(k)$ are also i.i.d with Gaussian distribution

$$W(k) \quad \sim \quad \mathcal{N}(0, \sigma_n^2) + j\mathcal{N}(0, \sigma_n^2) \tag{6.16}$$

Therefore the distribution of $Y(k)$ is given by

$$Y(k_0') \quad \sim \quad \mathcal{N}(\sqrt{NP_s}, \sigma_n^2) + j\mathcal{N}(0, \sigma_n^2) \tag{6.17}$$

$$Y(k) \quad \sim \quad \mathcal{N}(0, \sigma_n^2) + j\mathcal{N}(0, \sigma_n^2) \quad k \neq k_0' \tag{6.18}$$

Distribution of metric at correct offset (i.e. $k = k_0'$) :

At correct offset, the metric $C(k)$ is given by

$$C(k_0') = \left|\sqrt{NP_s} + W(k_0)\right|^2 = \left[\sqrt{NP_s} + W(k_0)\right]\left[\sqrt{NP_s} + W(k_0)\right]^* \quad (6.19)$$

$$= NP_s + |W(k_0)|^2 + \sqrt{NP_s}\left[W(k_0) + W^*(k_0)\right] \quad (6.20)$$

For high SNR, second term in above equation can be neglected and noting that the third term is nothing but $2Re\{W(k_0)\}$, we get

$$C(k_0') = NP_s + 2\sqrt{NP_s}Re\{W(k_0)\} \quad (6.21)$$

Therefore

$$C(k_0') \sim \mathcal{N}(NP_s, 4NP_s\sigma_n^2) = \mathcal{N}(NP_s, \frac{2NP_s^2}{SNR}) \quad (6.22)$$

where equality results from equation 6.11.

Distribution at incorrect timing instant (any $k \neq k_0'$) :

At incorrect offset the metric $C(k)$ will become

$$C(k_{inc}) = |W_1(k_{inc})|^2 \quad (6.23)$$

Therefore $C(k_{inc})$ has central chi square distribution with 2 degrees of freedom with mean and variance given by

$$E[C(k_{inc})] = 2\sigma_n^2 \quad (6.24)$$

$$var[C(k_{inc})] = 4\sigma_n^2 \quad (6.25)$$

Probability of Error (Pe) expression :

By Pe, we mean the probability that our estimate is not equal to actual IFO i.e. $Pe = P(\widehat{\triangle k_i} \neq \triangle k_i)$. Error will occur if we detect peak on incorrect offset i.e. $C(k_0') < C(k)$ for one or more $k \neq k_0'$. So it is easier first to find Probability of correct estimation (Pc) which is given by

$$
\begin{aligned}
Pc &= \int_0^\infty Pr(c > C(k), \forall k \neq k_0', k \text{ is even}/c) \cdot p(c) \cdot dc \\
&= \int_0^\infty [F_{c(k)}(c)]^{\frac{N}{2}-1} \cdot p(c) \cdot dc \quad for \, any \, k \neq k_0' \tag{6.26} \\
&= \frac{1}{\sqrt{2\pi\sigma_c^2}} \int_0^\infty \left(1 - e^{\left(-\frac{c}{2\sigma_n^2}\right)}\right)^{\frac{N}{2}-1} e^{\left(-\frac{(c-NP_s)^2}{8NP_s\sigma_n^2}\right)} \cdot dc \tag{6.27}
\end{aligned}
$$

where $C(k_0')$ is denoted by c for convenience, $p(c) = \frac{1}{\sqrt{2\pi\sigma_c^2}} exp(\frac{(c-E(c))^2}{2\sigma_c^2})$= pdf of c, $\sigma_c^2 = var(c) = 4NP_s\sigma_n^2$ by equation 6.22, F_r= CDF of r and is given by $F_r(c) = 1 - exp\left(-\frac{c}{2\sigma_r^2}\right)$. The i.i.d nature of $C(k)$ ($\forall k$) is used to derive equation 6.26. The Probability of error is given by

$$
Pe = 1 - Pc \tag{6.28}
$$

6.2.2 Data Model 2 : ISI Channel

Assume Exponential Rayleigh channel with tap coefficients having distribution

$$
h(l) \sim \mathcal{N}(0, 0.5\sigma_{hl}^2) + j\mathcal{N}(0, 0.5\sigma_{hl}^2) \quad \forall l = 0, \dots, L \tag{6.29}
$$

Expressions for $s(k)$, $x(t)$, and $w(n)$ are same as for AWGN case (see equation 6.8, 6.9, 6.10). However, $z(n)$ in this case is given by

$$
\begin{aligned}
z(t) &= x(t) * h(t) + w(t) \tag{6.30} \\
z(t) &= \frac{1}{\sqrt{N}} s(k_0) H(k_0) + w(t) \quad \forall t = 0, \dots, N-1 \tag{6.31}
\end{aligned}
$$

where $H(k_0) = \sum_{t=0}^{N-1} h(t)e^{-j2\pi k_0 t}$. Equation 6.31 arises from equations 6.9 and 6.30, and definition of $H(k_0)$. Therefore

$$
SNR = \frac{P_s \sum_{l=0}^L \sigma_{hl}^2}{2\sigma_n^2} \tag{6.32}
$$

After frequency offset, we get

$$
y(t) = z(t)e^{j2\pi t \triangle k_i/N} \tag{6.33}
$$

Taking FFT, we get

$$Y(k) = \begin{cases} s(k_0)H(k_0) + W(k_0) & k = k_0' \\ W_1(k) & k \neq k_0' \end{cases}$$

(6.34)

Distribution of metric at correct offset :

Since $Y(k_0')$ is sum of independent Gaussian random variables, it is Gaussian distributed as

$$Y(k_0') \sim \mathcal{N}(0, \frac{NP_s}{2}\sum_{l=0}^{L}\sigma_{hl}^2 + \sigma_n^2) + j\mathcal{N}(0, \frac{NP_s}{2}\sum_{l=0}^{L}\sigma_{hl}^2 + \sigma_n^2)$$

(6.35)

Let us denote $\sigma_c^2 \triangleq \frac{NP_s}{2}\sum_{l=0}^{L}\sigma_{hl}^2 + \sigma_n^2$ for convenience. So $C(k_0') = |Y(k_0')|^2$ will have central chi square pdf with two degrees of freedom with mean and variance given by following equations

$$E[C(k_0')] = 2\sigma_c^2$$

(6.36)

$$var[C(k_0')] = 4\sigma_c^4$$

(6.37)

Distribution of metric at incorrect offset :

At incorrect offset, $C(k_{inc}) = |W_1(k)|^2$, so distribution of metric at incorrect offset is same as for AWGN and mean and variance are given by equations 6.24 and 6.25.

Probability of error :

Probability of correct estimation Pc is same as for AWGN case (see equation 6.26) except that $p(c)$ in this case in central chi square instead of Gaussian in AWGN case i.e.

$$p(c) = \frac{1}{2\sigma_c^2}exp\left(-\frac{c}{2\sigma_c^2}\right)$$

(6.38)

Therefore equation for probability of correct decision in this case is given by

$$Pc = \frac{1}{2\sigma_c^2}\int_0^\infty \left(1 - e^{\left(-\frac{c}{2\sigma_n^2}\right)}\right)^{\frac{N}{2}-1} e^{\left(-\frac{c}{2\sigma_c^2}\right)} \cdot dc$$

(6.39)

and probability of error can be calculated as

$$Pe = 1 - Pc$$

(6.40)

$N \rightarrow$ SNR$\downarrow$ (in dB)	16	32	64	128
-4	1.58×10^{-1}	3.55×10^{-2}	1.59×10^{-3}	3.1×10^{-6}
0	1.06×10^{-2}	2.07×10^{-4}	7.35×10^{-7}	3×10^{-10}
4	1.71×10^{-4}	8×10^{-10}	6×10^{-11}	0
8	6.42×10^{-8}	0	0	0

Table 6.1: Pe for various values of SNR and N in AWGN scenario (theoretical)

$N \rightarrow$ SNR$\downarrow$ (in dB)	16	32	64	128
-4	1.52×10^{-1}	2.86×10^{-2}	5.9×10^{-4}	$< 10^{-5}$
0	4.06×10^{-2}	1×10^{-5}	$< 10^{-5}$	$< 10^{-5}$
4	$< 10^{-5}$	$< 10^{-5}$	$< 10^{-5}$	$< 10^{-5}$
8	$< 10^{-5}$	$< 10^{-5}$	$< 10^{-5}$	$< 10^{-5}$

Table 6.2: Pe for various values of SNR and N in AWGN scenario (simulation)

6.3   Simulation Results and Observation

AWGN Channel :

Tables 6.1 and 6.2 presents the simulated and theoretical values for Pe for various values of SNR and N for AWGN channel. For each SNR value, the simulation was run 10^5 times, each time generating different PN sequences, and noise. Cyclic prefix of 12 was used. BPSK modulation was used. For every realization, the frequency offset as well as subcarrier index on which impulse was sent, were changed. It can be seen that performance of the proposed tone based scheme is very good, even in low SNR and low N. It decreases monotonically with increasing SNR and with increasing N. The simulation and theoretical results are slightly mismatching for low values of SNR, but this can be explained by the fact that simplified theoretical expression (see equations 6.21 and 6.28) were obtained for high SNR values and the values obtained in tables are for low SNR. For High SNR values, they are approximately same.

ISI Channel :

Figure 6.1 shows (a) Pe Vs SNR and (b) Pe Vs N curves for Exponential decaying Rayleigh Channel (ISI) for simulation and theoretical cases. For each SNR value, the simulation was run 10^5 times, each time generating different PN sequences, channel realizations, and noise. Channel Order was L=5. Channel tap coefficients were normalized so that sum of variances of each tap was 1 i.e. $\sum_{l=0}^{L} \sigma_{hl}^2 = 1$. Cyclic Prefix length was 12. BPSK modulation was used. It can be seen that the simulation and theo-

(a) Pe Vs SNR   (b) Pe Vs N
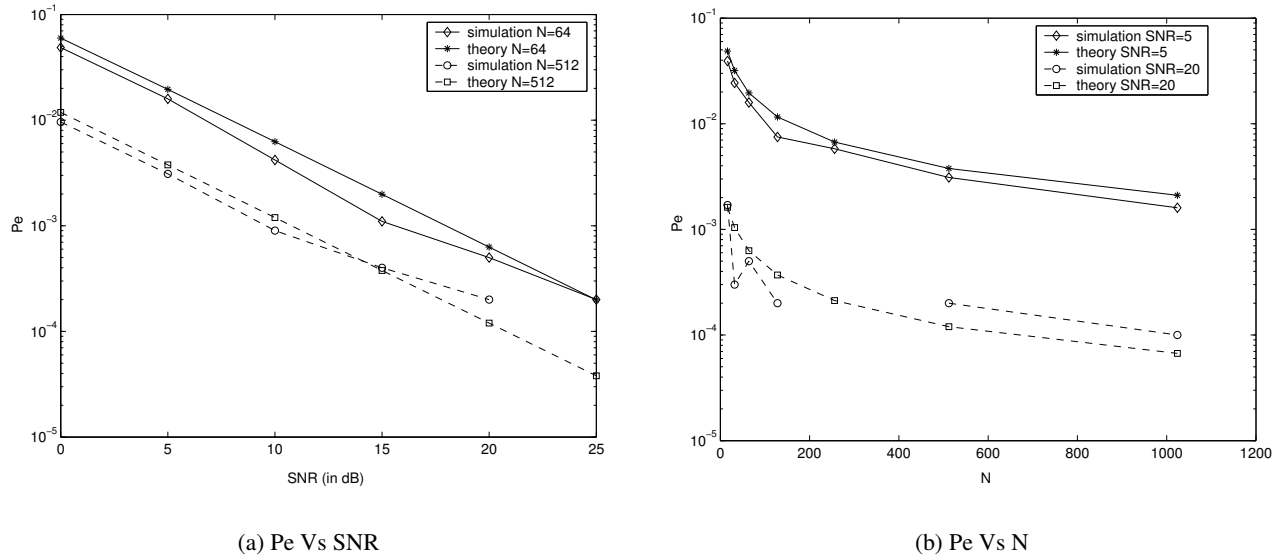
Figure 6.1: Pe curves for Exponential Rayleigh (ISI) channel

retical values from mathematical analysis are approximately same. The performance of the proposed tone based scheme is good in high SNR and high N. It decreases monotonically with increasing SNR and with increasing N. The performance of scheme has deteriorated as compared to its performance in AWGN, for which some modification has been proposed to improve the performance of this scheme in ISI conditions.

Effect of timing offset :

Figure 6.2 show the Pe curves for different timing offset (TO). Here '0' corresponds to exact start of data part in the training symbol. It can be seen that for TO between (-(CP-L) to 0 i.e. -6 to 0 in this case) has low Pe as compared to other offsets and Pe value is approximately same in this region.

6.4 Modification to the Proposed Scheme for ISI case (Multitone)

Whenever channel at subcarrier k_0 is bad i.e. $H(k_0)$ has small value, then the proposed tone based algorithm performs rather badly. To improve on this, we shall send data on more number of subcarriers in IFO training symbol, giving frequency diversity and hence a good performance. We will henceforth use notation Sm to denote case of Multitone scheme, in which data is sent on m subcarriers of IFO training symbol and rest of subcarriers will carry zeroes. The mathematical analysis has been performed for Sm. The cost to be paid is the frequency acquisition range is reduced by m. To get optimum frequency acquisition the subcarrier have to be kept equidistant from each other.
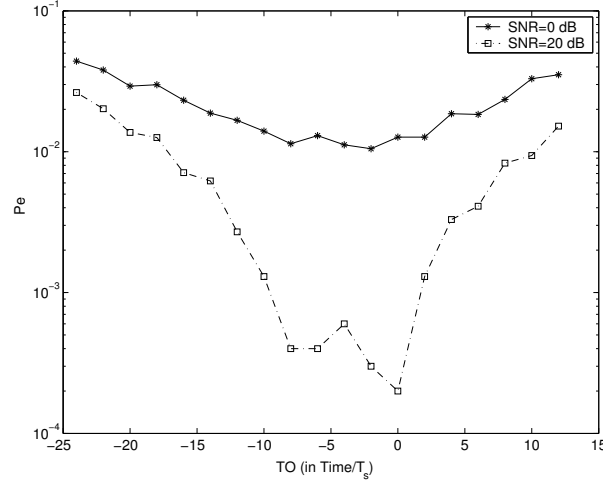
Figure 6.2: Pe vs Timing Offset

6.4.1 Mathematical Analysis

Data modulating the subcarriers of the IFO training symbol are

$$s(k) = \begin{cases} \sqrt{\frac{NP_s}{m}} & k = k_i \\ 0 & k \neq k_i \end{cases} \tag{6.41}$$

where k_i denote the subcarrier index on which data i.e. ($\sqrt{\frac{NP_s}{m}}$) is send in IFO training symbol, and it is given by $k_i = k_0 + \frac{iN}{m}$ and $i = 0, 1, \ldots, m-1$. Following the similar argument as in case of ISI for tone based scheme, at receiver we get

$$Y(k) = \begin{cases} s(k_i)H(k_i) + W(k_i) & k = k_i' \\ W_1(k) & k \neq k_i' \end{cases} \tag{6.42}$$

Metric is same as given by equation 6.4 i.e. begin_inset Formula \$C(k)=, but now $\widehat{\triangle k_i}$ is given as

$$k_{max} = arg\{\max_k C(k)\}$$
$$\widehat{\triangle k_i} = (k_{max} - k_0)mod(N/m) \tag{6.43}$$

Distribution of metric at correct offset :

Distribution of $Y(k)$ at correct offset can be obtained in similar way to ISI case for $S1$ and is given by

$$Y(k_0') \quad \sim \quad \mathcal{N}(0, \frac{NP_s}{2m}\sum_{l=0}^{L}\sigma_{hl}^2 + \sigma_n^2) + j\mathcal{N}(0, \frac{NP_s}{2m}\sum_{l=0}^{L}\sigma_{hl}^2 + \sigma_n^2) \qquad (6.44)$$

For convenience, denote $\sigma_{cm}^2 \triangleq \frac{NP_s}{2m}\sum_{l=0}^{L}\sigma_{hl}^2 + \sigma_n^2$. Then $C(k_0') = |Y(k_0')|^2$ will have a central chi square pdf with two degrees of freedom with mean and variance given by following equations

$$E[C(k_0')] \quad = \quad 2\sigma_{cm}^2 \qquad (6.45)$$

$$var[C(k_0')] \quad = \quad 4\sigma_{cm}^4 \qquad (6.46)$$

Distribution of metric at incorrect offset :

At incorrect offset, $C(k_{inc}) = |W_1(k)|^2$, so distribution of metric at incorrect offset is same as for AWGN and mean and variance are given by equations 6.24 and 6.25.

Probability of error :

Probability that metric at correct offset k_i (for $i = 0, 1, \ldots, m-1$) is greater than metric values at all incorrect offset (there are $\frac{N}{2} - m$ such offsets) is similar to equation 6.39 and is given by

$$Pc_i \quad = \quad \frac{1}{2\sigma_{cm}^2}\int_0^\infty \left(1 - e^{\left(-\frac{c_i}{2\sigma_n^2}\right)}\right)^{\frac{N}{2}-m} e^{\left(-\frac{c_i}{2\sigma_{cm}^2}\right)} \cdot dc_i \qquad i = 0, 1, \ldots, m-1$$

where $c_i \triangleq C(k_i')$ for convenience. Therefore Probability that metric at correct offset k_i is less than metric value at one or more of the incorrect offsets, will be given by

$$Pe_i \quad = \quad 1 - Pc_i \qquad i = 0, 1, \ldots, m-1$$

Now our estimation of IFO will go into error only if both $C(k_i)$ for $i = 0, 1, \ldots, m-1$ are less than some $C(k)$ $k \neq k_i$. Therefore probability of error for Sm will be given by

$$Pe_{sm} \quad = \quad Pe_0 \cdot Pe_1 \cdot \ldots \cdot Pe_{m-1} = (Pe_0)^m \qquad \because i.i.d \qquad (6.47)$$

Now it has been observed numerically that for various SNR values

$$Pe_{s1} < Pe_0 \quad \leq \quad mPe_{s1} \tag{6.48}$$

where Pe_{s1} is probability of error for $S1$ and is given by equation 6.40. The first inequality is logical, since now strength of impulse has reduced by factor of m (for Sm) as compared to $S1$. As SNR increases Pe_0 moves toward upperbound. From equations 6.47 and 6.48, we get upperbound on Pe_{sm}, which is given by

$$Pe_{sm} \quad \leq \quad (mPe_{s1})^m \tag{6.49}$$

Solving for $Pe_{sm} \leq (mPe_{s1})^m \leq Pe_{s1}$ we will get the values of Pe_{s1}, for which scheme will perform better for Sm as compared to $S1$. The expression for required Pe_{s1} is

$$Pe_{s1} \quad \leq \quad m \cdot exp(\frac{m}{1-m}) \tag{6.50}$$

which turns out to be $Pe_{s1} \leq 1$ for values of $m > 3$. Since Pe cannot be greater than 1, the performance will be better for every Pe_{s1} (even for $m = 4$). For $m = 2$, $Pe_{s1} \leq 0.27$ and for $m = 2$ $Pe_{s1} \leq 0.69$ which is true even for low N and low SNR.

6.4.2 Simulation Results and Observation

Figure 6.3 shows simulation results for $S1$, $S2$ and $S4$. Simulation parameters were similar to $S1$, except that IFO here was limited to the new acquisition range. For each SNR value, the simulation was run 10^5 times, each time generating different PN sequences, channel realizations, and noise. It can be seen that performance has greatly improved. Performance of Multitone scheme goes on improving as m increases but the acquisition range is reduced by the same factor. Hence there is trade off between acquisition range and Pe. In general, $m = 4$ should be sufficient as it gives good performance at low SNR and low N and acquisition range is one-fourth of OFDM bandwidth.

6.5 Comparison between the proposed schemes and existing schemes

Multitone is general case. For comparison with existing scheme it is used (except for performance in AWGN scenario where Single tone is sufficient).
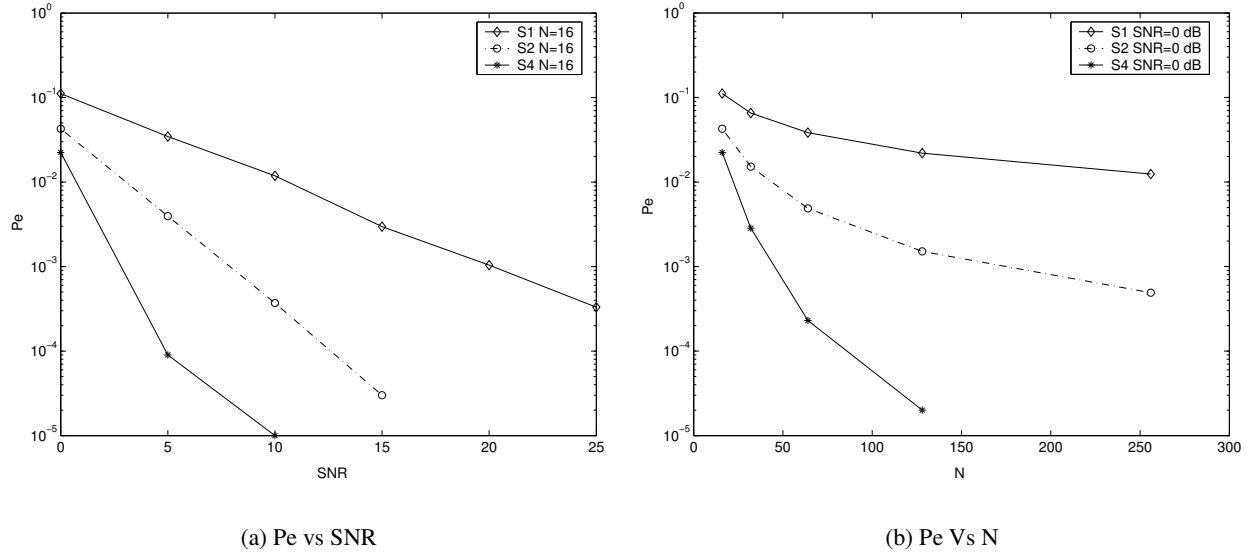
(a) Pe vs SNR

(b) Pe Vs N

Figure 6.3: Comparison of Multitone scheme for $S1$, $S2$, and $S4$

(a) Pe Vs SNR

(b) Pe vs N
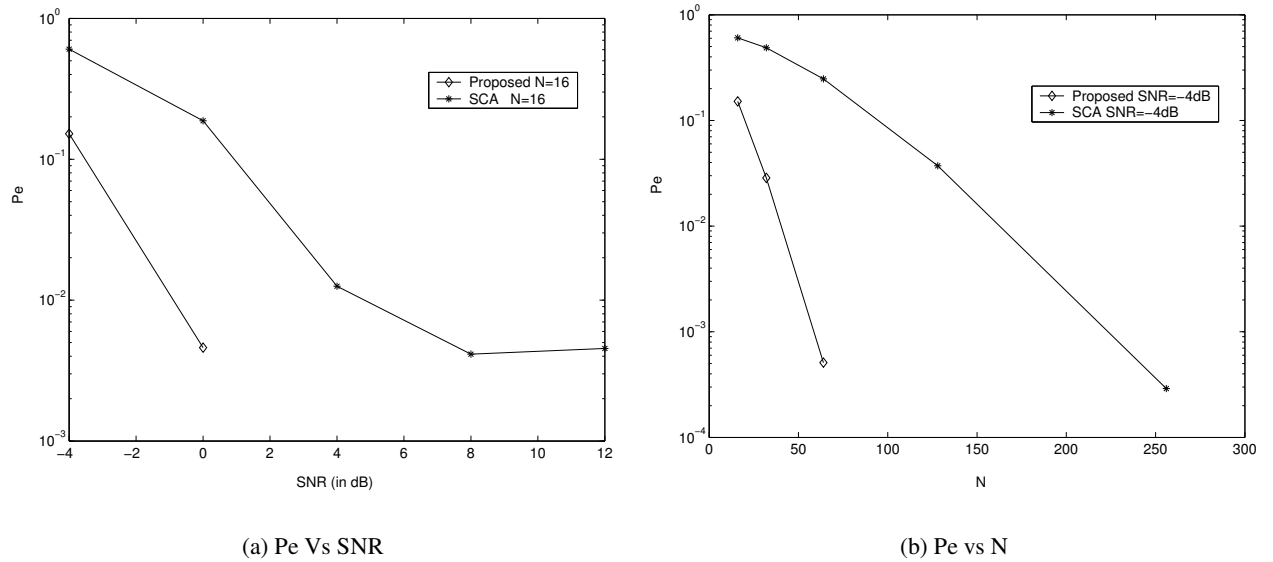
Figure 6.4: Pe Curves for Tone based scheme and SCA for different values of SNR and N in AWGN conditions

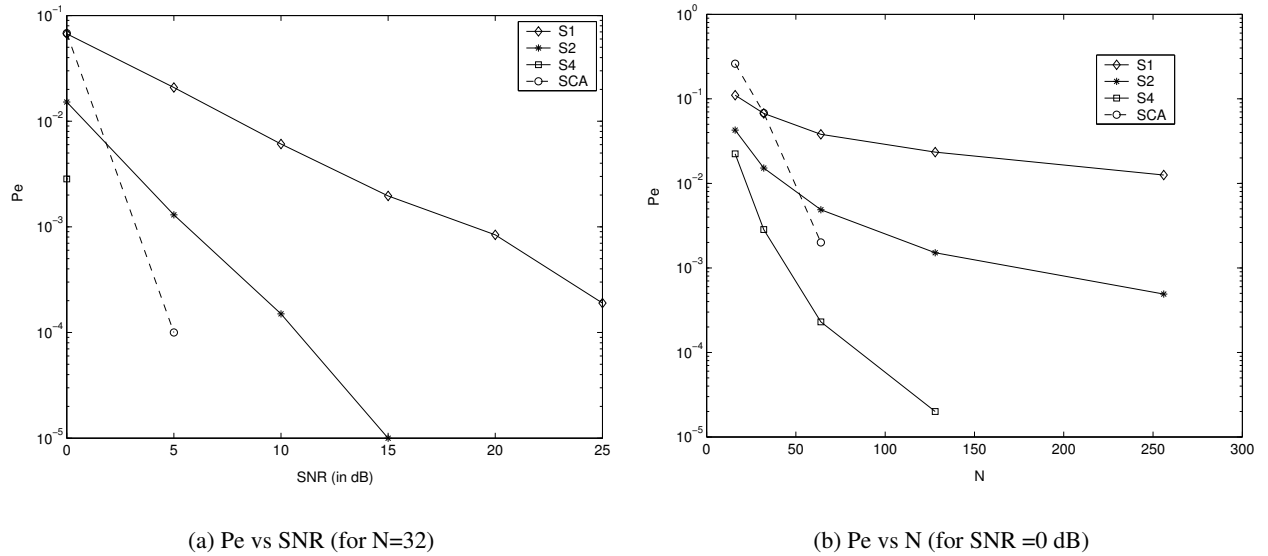(a) Pe vs SNR (for N=32)   (b) Pe vs N (for SNR =0 dB)

Figure 6.5: Pe Curves for Multitone scheme and SCA for different values of SNR and N for exponential decaying Rayleigh channel

6.5.1 Performance

AWGN Case :

Figure 6.4 shows Pe curves for the proposed scheme and SCA frequency offset estimation for AWGN scenario. Simulation parameters were similar to $S1$, except that IFO here was kept limited to the new acquisition range. For each SNR value, the simulation was run 10^5 times, each time generating different PN sequences, channels, and noise. Subcarrier Index on which impulse was sent, was kept changing in allowed range $0 \leq k_0 < N$, and k_0 is even. It was seen that performance of proposed scheme ($S1$) is better than that of SCA.

ISI Case

Figure 6.5 shows the Pe curves for the Multitone scheme and SCA frequency offset estimation for ISI scenario. Except for the channel model, simulation scenario is similar to that for AWGN case mentioned above. It was observed that for high SNR and high N, the performance of SCA is better than $S1$ and $S2$, but the performance is comparable with $S4$.

From the above figure, we don't get much idea about comparison of SCA and Multitone scheme with $S4$ at high N and SNR. For these values of N and SNR, Pe values are very low. Simulating for such condition involves enormous computation complexity. So we tried to analytically compare them on basis of their Pe equations. Pe equation for SCA IFO is similar to proposed tone based scheme for AWGN case (see equations 6.27 and 6.28) except that distributions at correct offset will be now given by equations 5.17,5.18 and distribution at incorrect offset will now be given by equations 5.19 and

(a) Pe vs SNR for N=32

(b) Pe vs N for SNR=10 dB
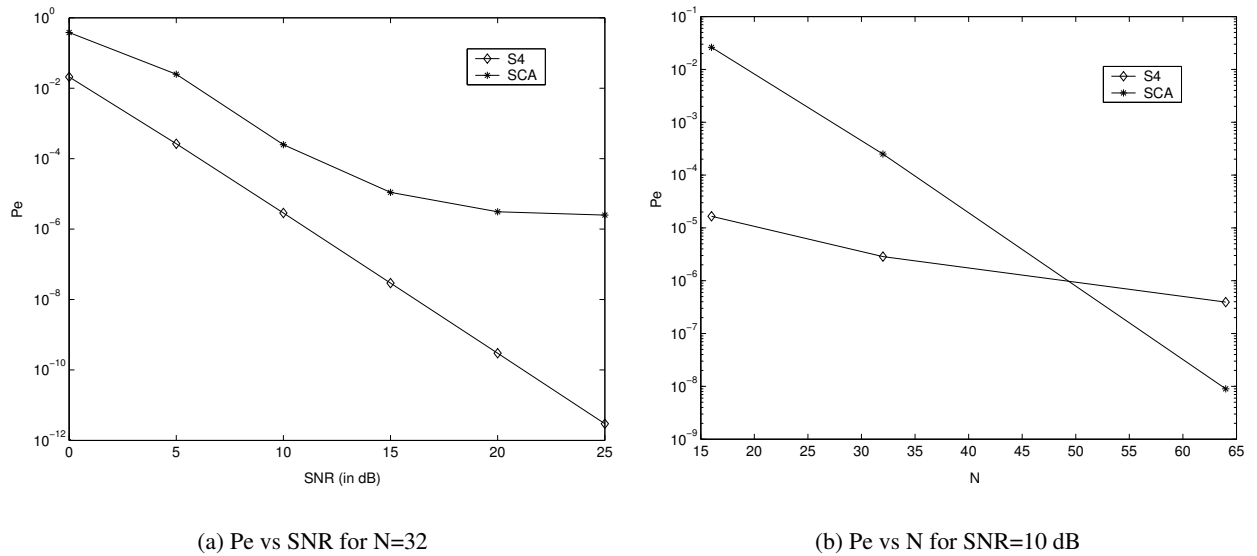
Figure 6.6: Theoretical Pe curves for SCA and Multitone scheme $S4$

Operation	SCA	Proposed
complex multiplication	$0.5 \cdot N^2 + N$	–
complex division	$N/2$ (for vk)	–
complex addition	$N^2/2$	–
real division	1	1 (mod operation)

Table 6.3: Relative Computation Complexity for SCA and Proposed Scheme

5.20. So numerically Pe values where obtained for SCA and $S4$. Values of Pe for $S4$ is calculated from equation 6.47. The corresponding plots are shown in figure 6.6. One thing worth noting from these plots is that Pe decreases exponentially with increase in SNR (dB) in case of Multitone scheme but same is not true in case of SCA (even though there is monotonic decrease, but the rate is slow). On other hand Pe decreases exponentially with increasing N in case of SCA and the rate of decrease is low in case of Multitone scheme with increase in N.

6.5.2 Computation Complexity

We have calculated the computational complexity for SCA IFO estimation from equation 5.14. Similarly for the Multitone scheme (which is general case), computational complexity is calculated from equation 6.4. Table 6.3 summarizes relative computational complexities between SCA and proposed scheme for IFO estimation. By relative computation complexity we mean that the computations common to both have been ignored (calculating $N/2$ absolute square quantities). It can be seen that the proposed scheme has very low complexity.

6.5.3 Frequency Acquisition Range

The Frequency Acquisition range for SCA is total OFDM bandwidth, and in case of Multitone scheme the range is total bandwidth divided by m. But for small values of $m = 1$ to 16, it is still a big range because most standards have frequency offset of at most few subcarrier spacings. For 802.11a WLAN standard, maximum frequency offset is 50 ppm at 5 GHz carrier frequency and 250 KHz subcarrier spacing. For this values, maximum frequency offset turns out to be 250 KHz i.e. one subcarrier spacing.

6.5.4 Number of Training symbol required

Case I. For Multitone scheme, no additional symbol is required for timing synchronization and fractional frequency offset estimation. But we will require an additional symbol for channel estimation.

Case II. We can perform timing synchronization and fractional frequency offset estimation using first of the two SCA training symbols. For the second training symbol, if we put data on odd subcarriers, we can apply proposed scheme on even subcarriers. The channel estimation can be carried out using even subcarriers of first training symbol and odd subcarriers of second training symbol.

Hence in both cases, we require at least 2 training symbols for timing synchronization, frequency offset correction and channel estimation.

6.6 Performance of Multitone scheme for timing synchronization and fractional frequency offset

This section aims at evaluating the performance of timing synchronization and fractional frequency offset estimation using SCA in conjunction with IFO training symbol (Case I of section 6.5.4). Simulations have been performed for $N = 1024$ in AWGN case to check whether the performance of the the proposed training symbol will work accurately. Figure 6.7 shows mean and variance at correct timing region (point inside plateau). Figure 6.8 shows mean and variance at instant outside the plateau. Figure 6.9 shows variance of error in estimating fractional frequency offset. From all these figures, it can be concluded that the SCA work satisfactorily for IFO training symbol, in respect of timing synchronization and fractional frequency offset estimation.
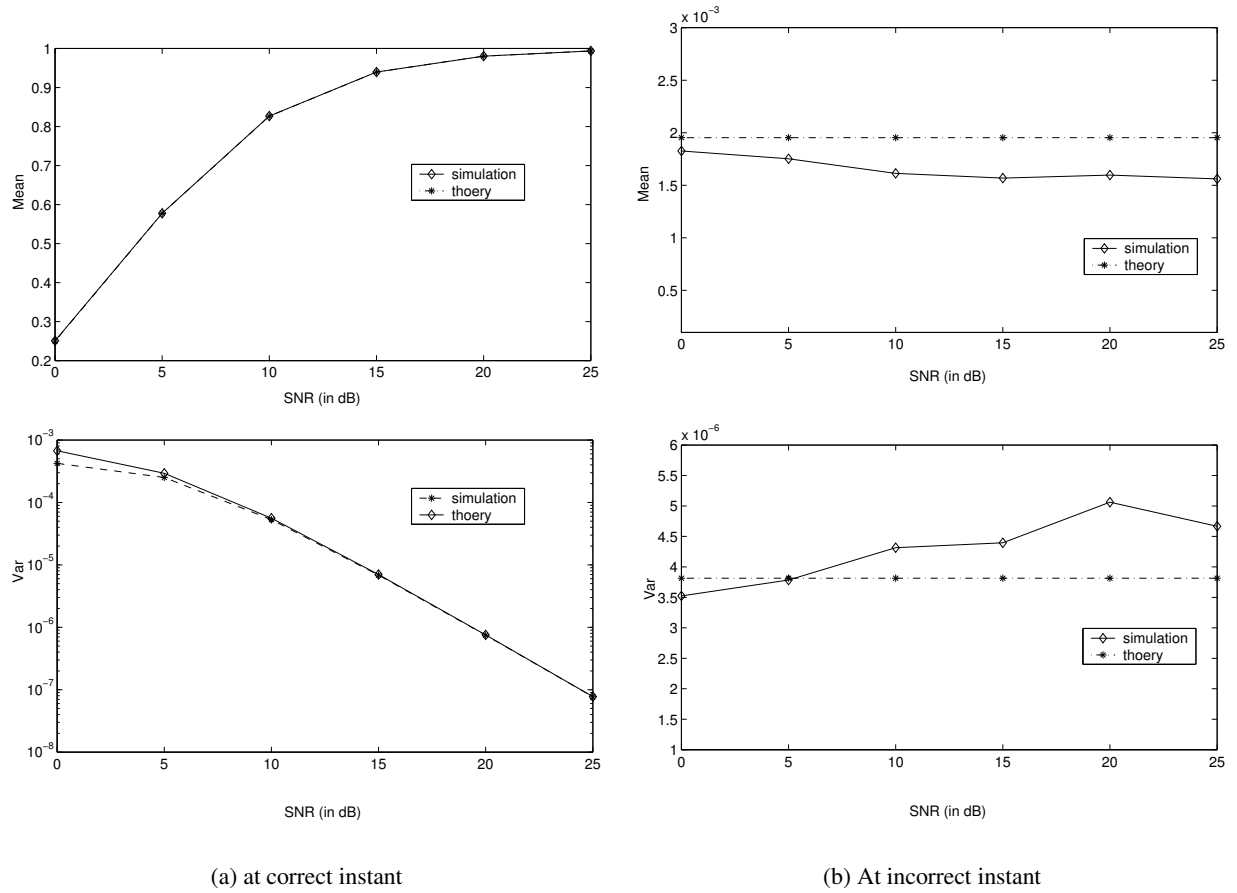
(a) at correct instant

(b) At incorrect instant

Figure 6.7: Mean and Variance at correct and incorrect timing instant for $N = 1024$ and AWGN case, $m = 4$.

(a) mean vs SNR
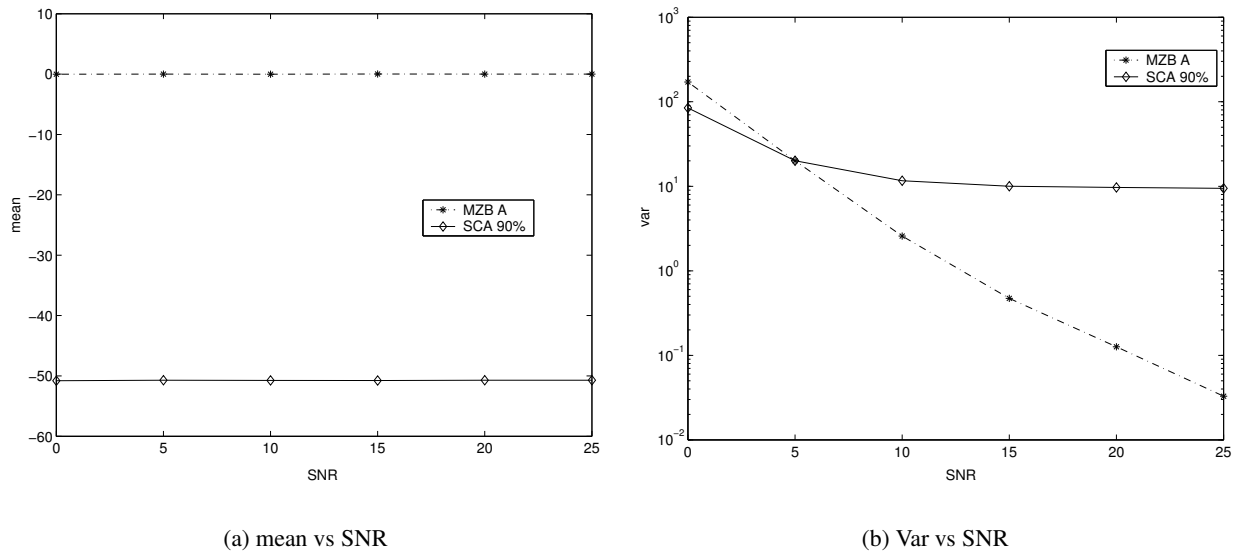
(b) Var vs SNR

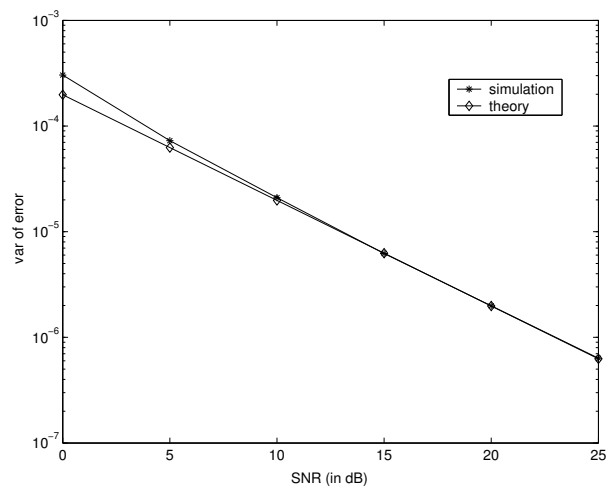Figure 6.8: mean and variance at correct timing instant

Figure 6.9: Variance of Fractional FO error

Chapter 7

Conclusions

In the early part of this work, dependency of PAPR on input constellation (through γ_c) was derived and corresponding expression for P_w was obtained for general constellations. Using this it was shown that PAPR for QAM is more than that for PSK of any order. A Pulse shaping scheme for PAPR reduction was also proposed. An analytical expression for reduction in upperbound on PAPR was obtained for the same.

In subsequent part, IOFDM was reviewed from PAPR reduction point of view for constant code rate. IOFDM was shown to be Superset of OFDM and SC-FDE. Trade-off can be achieved OFDM and SC-FDE by changing P (interleaving factor of IOFDM). BOFDM was proposed (structure similar to IOFDM but without interleaving and minor differences). It was shown that BOFDM is also superset of OFDM and SC-FDE. Later it was shown that BOFDM has more complexity than IOFDM. Performances of SLM, PTS, and IOFDM were compared and it was found that IOFDM is better than the other two schemes with respect to complexity, PAPR reduction, and amount of redundancy added.

Two Synchronization algorithms (1) SCA and (2) MZB were studied and implemented and a new scheme was proposed for IFO estimation which is simple and highly computationally efficient as compared to the existing schemes. A detailed mathematical analysis was carried out and Probability of error (Pe) expression for ISI and AWGN channel was derived. A modification (Multitone) was suggested which greatly improves the performance of the scheme even in low N and low SNR condition for ISI channel, but at the cost of reduced frequency acquisition range. General expression Pe_{sm}, i.e. Probability of error for Sm was also derived. An upperbound has been obtained on Pe_{sm} in terms of Pe_{s1}. The expression for range of values of Pe_{s1} for which Pe_{sm} will be less than Pe_{s1} (performance of m subcarrier case was better than 1 subcarrier case), is obtained. It was observed that for $m > 3$, the performance of Sm case will be better than that of $S1$ case.

Future Directions

In case of input stream consisting of binary sequences of different probabilities, PAPR can be reduced by assigning sequences with low probabilities to symbols in constellation with high power.

This will shift the CCDF curves for PAPR to left. But the probability assignment does not seem to be trivial. It changes average power of constellation resulting in change in upper bound on P_i. So optimum allocation of sequences to the constellation symbols according to their probabilities is open problem.

Bibliography

[1] Z.Wang and G.B.Giannakis, *Wireless multicarrier Communications : Where Fourier meets Shannon* IEEE SP magazine 2001.

[2] R.van Nee and Ramjee Prasad, *OFDM for Wireless Multimedia Communication,* Norwood, MA:Archtech House,2000.

[3] J.G.Proakis, D.G.Manolakis, *Digital Signal Processing*, Prentice Hall 1997.

[4] J.G.Proakis, *Digital Communication*, McGraw Hill 2001.

[5] V.G.S.Prasad, *Multiple Input Multiple Output techniques for Interleaved Orthogonal Frequency Division Multiplexing*, Masters Thesis, Department of Electrical Communication Engineering, Indian Institute of Science, January 2002.

[6] V.G.S.Prasad, K.V.S.Hari, *Interleaved Orthogonal Frequency Division Multiplexing (IOFDM) system* , IEEE Transaction on Signal Processing, Vol No.52, No.6, June 2004.

[7] Karthik Subramaniam, *Alternative Interleaving Schemes for Interleaved Orthogonal Frequency Division Multiplexing*, MSc Thesis, Department of Electrical Communication Engineering, Indian Institute of Science, August 2003.

[8] L.Litwin, M.Pugal, *The Principles of OFDM*, RF Signal Processing, January 2001.

[9] J.H.Manton, *Dissecting OFDM : The Independent Roles of the Cyclic Prefix and IDFT operation*, IEEE Communication Letters, Vol.5, No.12, December 2001.

[10] G.B.Giannakis, P.Duhamel, Z.Wang, *Cyclic Prefixing Or Zero-Padding for Wireless Multicarrier Communication?,* IEEE Transaction on communications, August 2001.

[11] C.Tellumbura, *Upper Bound on Peak Factor of N carriers system* , Electronics Letters, Vol no.33, No.19, September 1997.

[12] C.Tellumbura, *Phase optimization criterion for reducing Peak to Average Ratio in OFDM*, Electronic Letters vol. no.34, no.2, January 1998.

[13] S.H.Muller, J.B.Huber, *OFDM with reduced peak to power ratio by optimum combination of partial transmit sequences,* Electronic Letters vol.33, No.5, February 1997.

[14] R.Buaml, J.Huber, *Reducing the Peak to Average Power Ratio of multicarrier modulation by Selected Mapping*, Electronic Letters Vol 32, No.22, October 1996.

[15] S.H.Muller, J.B.Huber, *A Comparison of Peak Power Reduction Sequences for OFDM* , Global Telecommunications Conference, 1997. GLOBECOM '97., IEEE ,Volume: 1 , 3-8 Nov. 1997

[16] A.D.S.Jayalath, C.Tellambura, *The use of Interleaving to reduce the Peak to Average Power Ratio of an OFDM signal* , Global Telecommunications Conference, 2000. GLOBECOM '00. IEEE ,Volume: 3 , 27 Nov.-1 Dec. 2000

[17] S.B.Slimane, *Peak to Average Power ratio reduction by Pulse Shaping.* Global Telecommunications Conference, 2000. GLOBECOM '00. IEEE ,Volume: 3 , 27 Nov.-1 Dec. 2000

[18] D.Falconer, B.Eidson, *Frequency Domain Equalization for Single Carrier Broadband Wireless Systems*, IEEE Communication Magazine, April 2002.

[19] H.Sari, G.Karam, J.Jeanclaude, *Transmission Technique for digital terrestrial TV broadcasting*, IEEE Communication Magazine 1995.

[20] M.J.E.Golay, *Golay complementary series, IRE Transactions on Information Theory* , Vol.IT-7, April 1961.

[21] J.Jedwab, J.A.David, *Peak to mean power control in OFDM, Golay complementary sequences, and Reed Muller codes*, IEEE Transactions on Information Theory, Vol.45. No.7, November 1999.

[22] T.M.Schmidl, D.C.Cox, *Robust Frequency and Timing Synchronization for OFDM ,* IEEE Trans. Commun., vol 45, pp 1613-1621 Dec 1997.

[23] H.Minn, M.Zeng, V.K.Bhargava, *On Timing Offset Estimation for OFDM Systems,* IEEE Communication Letters, Vol 4, No.7, July 2000.

[24] P.H.Moose *A Technique for Orthogonal Frequency Division Multiplexing frequency offset correction,* IEEE Trans. on Commun., Vol 42. No.10, pp 2908-2914, Oct 1994.

[25] Jian Li, G.Liu, G.B.Giannakis, *Carrier Frequency Offset Estimation for OFDM based WLANs.* IEEE Signal Processing Letters, Vol 8, No.3, pp 80-82, March 2001.

[26] Kalyan.K.G, *Synchronization Algorithms for OFDM based Systems,* Masters Thesis, Department of Electrical Communication, Indian Institute of Science, Jan 2003.

[27] H.Koyabashi, *A Novel Symbol Frame and Carrier Frequency Synchronization for Burst Mode OFDM Signal.* VTC-2000.

[28] D.Rife and R.Boorstyn, *Single Tone Parameter Estimation from discrete time observation,* IEEE Trans. Inform. Theory, Vol. IT-20, pp 591-598, Sept. 1974.